
On the Identification of Temporally Causal Representation with Instantaneous Dependence

Zijian Li^{3,*}, Yifan Shen^{3,*}, Kaitao Zheng², Ruichu Cai^{2,†}, Xiangchen Song^{3,1}, Mingming Gong^{3,6},
Zhifeng Hao⁴, Zhengmao Zhu⁵, Guangyi Chen^{3,1}, Kun Zhang^{3,1,†}

¹ Carnegie Mellon University

² School of Computer Science, Guangdong University of Technology

³ Mohamed bin Zayed University of Artificial Intelligence

⁴ Shantou University

⁵ Nanjing University

⁶ University of Melbourne

Abstract

Temporally causal representation learning aims to identify the latent causal process from time series observations, but most methods require the assumption that the latent causal processes do not have instantaneous relations. Although some recent methods achieve identifiability in the instantaneous causality case, they require either interventions on the latent variables or grouping of the observations, which are in general difficult to obtain in real-world scenarios. To fill this gap, we propose an **ID**entification framework for instantane**O**us Latent dynamics (**IDOL**) by imposing a sparse influence constraint that the latent causal processes have sparse time-delayed and instantaneous relations. Specifically, we establish identifiability results of the latent causal process based on sufficient variability and the sparse influence constraint by employing contextual information of time series data. Based on these theories, we incorporate a temporally variational inference architecture to estimate the latent variables and a gradient-based sparsity regularization to identify the latent causal process. Experimental results on simulation datasets illustrate that our method can identify the latent causal process. Furthermore, evaluations on multiple human motion forecasting benchmarks with instantaneous dependencies indicate the effectiveness of our method in real-world settings.

1 Introduction

Time series analysis [1–5], which has been found widespread applications across diverse fields such as weather [6, 7], finance [8, 9], and human activity recognition [10, 11], aims to capture the underlying patterns [12, 13] behind the time series data. To achieve this goal, one solution is to estimate the latent causal processes [14–16]. However, without further assumptions [17, 18], it is challenging to identify latent causal processes, i.e., ensure that the estimated latent causal process is correct.

Researchers have exploited Independent Component Analysis (ICA) [19–22], where observations are generated from latent variables via a linear mixture function, to identify the latent causal process. To deal nonlinear cases, different types of assumptions including sufficient changes [23–25] and structural sparsity [26, 27] are proposed to meet the independent change of latent variables. Specifically, several works leverage auxiliary variables to achieve strong identifiable results of latent variables [28, 29, 18, 30, 24, 31]. To seek identifiability in an unsupervised manner, other researchers [32, 33] propose the structural sparsity on the generation process from latent sources to observation. However,

*Equal contributions

†Corresponding authors.

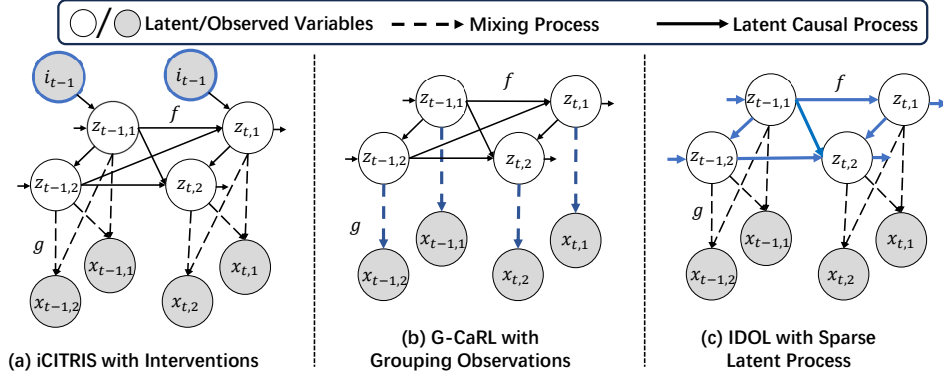


Figure 1: Three different data generation processes with time-delayed and instantaneous dependencies. (a) iCITRIS [34] requires intervention variables \mathbf{i}_t for latent variables (the gray nodes with blue rim.). (b) G-CaRL [35] assumes that observed variables can be grouped according to which latent variables they are connected to (the blue dotted lines), (c) IDOL requires a **sparse** latent causal process (the blue solid lines), which is close to real-world scenarios.

these methods usually do not have instantaneous relations, e.g., the latent variables are mutually independent conditional on their time-delayed parents at previous timestamps. Hence, further assumptions are used for identifiability. For example, Lippe et al. [34] demonstrate identifiability by assuming that there exist interventions on latent variables, and Morioka et al. [35] yield identifiability with the assumption of the grouping of observational variables. Recently, Zhang et al. [36] use the sparse structures of latent variables to achieve identifiability of static data under distribution shift. Beyond it, in this work, we demonstrate that temporal identifiability benefits from the sparsity constraint on the causal influences in the latent causal processes by employing the temporal contextual information, i.e., the variables across multiple timestamps. Please refer to Appendix A1 for further discussion of related works, including the identification of latent variables and instantaneous time series.

Although these methods [34, 35] have demonstrated the identifiability of latent variables with instantaneous dependencies, they often impose strict assumptions on the latent variables and observations. Specifically, as shown in Figure 1 (a), iCITRIS [34] reaches identifiability by assuming that interventions \mathbf{I}_t , i.e., the gray nodes with blue rim, on the latent variables, which is expensive and difficult in practice. For instance, considering the joints as the latent variables of a human motion process, it is almost impossible to intervene in the joints of the knee when a human is walking. Moreover, as shown in Figure 1 (b), G-CaRL [35] employs the grouping of observations to identify the latent variables, i.e., the blue dotted lines. However, the grouping of observations is usually expensive, for example, grouping the sensors on a human body from the joints of skeletons requires massive of expert knowledge and labor. Therefore, it is urgent to find a more general approach with an appropriate assumption to identify the latent causal process with instantaneous dependencies.

To identify the latent variables in a more relaxed assumption that is applicable to real-world time series data, we present a general **Identification framework for instantaneous Latent dynamics (IDOL)** with the only assumption of the sparse causal influences in the latent process named “sparse latent process” as shown in Figure 1 (c), where the transition process denoted by the blue solid lines is sparse. It is worth noting that the sparse latent process assumption is common and naturally appears in many practical time series data. In the example of human motion forecasting, a skeleton of the human body, which can be considered to be a latent causal process, is usually sparse, for example, the changes of arms and legs can be treated as independent. Based on the *latent process sparsity*, we first establish the relationship between the ground truth and the estimated latent variables by employing sufficient variability. Sequentially, we propose the sparse latent process assumption to achieve the component-wise identifiability of latent variables by leveraging the contextual information of time series data. Building upon this identifiability framework, we develop the **IDOL** model, which involves a temporally variational inference neural architecture to reconstruct the latent variables and a gradient-based sparsity penalty to encourage the sparse causal influences in the latent process for identifiability. Evaluation results on the simulation datasets support the theoretical claims and experiment results on several benchmark datasets for time series forecasting highlight the effectiveness of our method.

2 Problem Setup

2.1 Time Series Generative Model under Instantaneous Latent Causal Process

We begin with the data generation process as shown in Figure 1 (c), where the latent causal process is sparse. Suppose that we have time series data with discrete timestamps $\mathbf{X} = \{\mathbf{x}_1, \dots, \mathbf{x}_t, \dots, \mathbf{x}_T\}$, where \mathbf{x}_t is generated from latent variables $\mathbf{z}_t \in \mathcal{Z} \subseteq \mathbb{R}^n$ via an invertible and nonlinear mixing function \mathbf{g} , which is shown in Equation 1,

$$\mathbf{x}_t = \mathbf{g}(\mathbf{z}_t). \quad (1)$$

Specifically, the i -th dimension of the latent variable $z_{t,i}$ is generated via the latent causal process, which is assumed to be related to the time-delayed parent variables $\text{Pa}_d(z_{t,i})$ and the instantaneous parents $\text{Pa}_e(z_{t,i})$, respectively. Formally, it can be written via a structural equation model [37] as

$$z_{t,i} = f_i(\text{Pa}_d(z_{t,i}), \text{Pa}_e(z_{t,i}), \epsilon_{t,i}) \quad \text{with} \quad \epsilon_{t,i} \sim p_{\epsilon_i}, \quad (2)$$

where $\epsilon_{t,i}$ denotes the temporally and spatially independent noise extracted from a distribution p_{ϵ_i} . To better understand this data generation process, we take an example of human motion forecasting, where the joint positions can be considered as latent variables. In this case, the rigid body effects among joints result in instantaneous effects, and the kinematic representations like relative joint angles between limbs recorded from the sensors on the human body are observed variables that are the mixtures of joint positions. Therefore, we can consider the process from latent joint positions to the observed kinematic representations as the mixing process.

2.1.1 Identifiability of Latent Causal Processes

Based on the aforementioned generation process, we further provide the definition of the identifiability of latent causal process with instantaneous dependency in Definition 1. Moreover, if the estimated latent processes can be identified at least up to permutation and component-wise invertible transformation, the latent causal relations are also immediately identifiable because conditional independence relations fully characterize instantaneous causal relations in an instantaneous causally sufficient system, where there are no causal confounders in the latent causal processes.

Definition 1 (Identifiable Latent Causal Process). *Let $\mathbf{X} = \{\mathbf{x}_1, \dots, \mathbf{x}_T\}$ be a sequence of observed variables generated by the true latent causal processes specified by $(f_i, p(\epsilon_i), \mathbf{g})$ given in Eq 1 and 2. A learned generative model $(\hat{f}_i, \hat{p}(\epsilon_i), \hat{\mathbf{g}})$ is observational equivalent to $(f_i, p(\epsilon_i), \mathbf{g})$ if the model distribution $p_{\hat{f}_i, \hat{p}(\epsilon_i), \hat{\mathbf{g}}}(\{\mathbf{x}\}_{t=1}^T)$ matches the data distribution $p_{f_i, p(\epsilon_i), \mathbf{g}}(\{\mathbf{x}\}_{t=1}^T)$ for any value of \mathbf{x}_t . We say latent causal processes are identifiable if observational equivalence can lead to a version of generative process up to a permutation π and component-wise invertible transformation \mathcal{T} :*

$$p_{\hat{f}_i, \hat{p}(\epsilon_i), \hat{\mathbf{g}}}(\{\mathbf{x}\}_{t=1}^T) = p_{f_i, p(\epsilon_i), \mathbf{g}}(\{\mathbf{x}\}_{t=1}^T) \Rightarrow \hat{\mathbf{g}} = \mathbf{g} \circ \pi \circ \mathcal{T}. \quad (3)$$

Once the mixing process gets identified, the latent variables will be immediately identified up to permutation and component-wise invertible transformation:

$$\hat{\mathbf{z}}_t = \hat{\mathbf{g}}^{-1}(\mathbf{x}_t) = (\mathcal{T}^{-1} \circ \pi^{-1} \circ \mathbf{g}^{-1})(\mathbf{x}_t) = (\mathcal{T}^{-1} \circ \pi^{-1})(\mathbf{g}^{-1}(\mathbf{x}_t)) = (\mathcal{T}^{-1} \circ \pi^{-1})(\mathbf{z}_t). \quad (4)$$

Furthermore, with identified latent variables, the whole causal process within latent variables can also be determined since intervention can be applied to any single variable easily.

3 Identification Results for Latent Causal Process

Given the definition of identification of latent causal process, we show how to identify the latent causal process in Figure 1 (c) under a sparse latent process. Specifically, we first leverage the connection between conditional independence and cross derivatives [38] and the sufficient variability of temporal data to discover the relationships between the estimated and the true latent variables, which is shown in Theorem 1. Moreover, we establish the identifiability result of latent variables by enforcing the sparse causal influences, as shown in Theorem 2. Finally, we also show that the existing identifiability results of the temporally causal representation learning methods are a special case of our **IDOL** method, which is shown in Corollary 2.1.

3.1 Relationships between Ground-truth and Estimated Latent Variables

In this section, we figure out the relationships between ground truth and estimated latent variables under a temporal scenario with instantaneous dependence. In order to incorporate contextual information to aid in the identification of latent variables \mathbf{z}_t , latent variables of L consecutive timestamps including \mathbf{z}_t , are taken into consideration. Without loss of generality, we consider a simplified case, where the length of the sequence is 2, i.e., $L = 2$, and the time lag is 1, i.e., $\tau = 1$. Please refer to Appendix A2.2 for the general case of multiple lags and sequence lengths

Theorem 1. *For a series of observations $\mathbf{x}_t \in \mathbb{R}^n$ and estimated latent variables $\hat{\mathbf{z}}_t \in \mathbb{R}^n$ with the corresponding process $\hat{f}_i, \hat{p}(\epsilon), \hat{g}$, where \hat{g} is invertible, suppose the process subject to observational equivalence $\mathbf{x}_t = \hat{\mathbf{g}}(\hat{\mathbf{z}}_t)$. Let $\mathbf{c}_t \triangleq \{\mathbf{z}_{t-1}, \mathbf{z}_t\}$ and $\mathcal{M}_{\mathbf{c}_t}$ be the variable set of two consecutive timestamps and the corresponding Markov network respectively. Suppose the following assumptions hold:*

- *A1 (Smooth and Positive Density): The probability function of the latent variables \mathbf{c}_t is smooth and positive, i.e., $p_{\mathbf{c}_t}$ is third-order differentiable and $p_{\mathbf{c}_t} > 0$ over \mathbb{R}^{2n} ,*
- *A2 (Sufficient Variability): Denote $|\mathcal{M}_{\mathbf{c}_t}|$ as the number of edges in Markov network $\mathcal{M}_{\mathbf{c}_t}$. Let*

$$w(m) = \left(\frac{\partial^3 \log p(\mathbf{c}_t | \mathbf{z}_{t-2})}{\partial c_{t,1}^2 \partial z_{t-2,m}}, \dots, \frac{\partial^3 \log p(\mathbf{c}_t | \mathbf{z}_{t-2})}{\partial c_{t,2n}^2 \partial z_{t-2,m}} \right) \oplus \left(\frac{\partial^2 \log p(\mathbf{c}_t | \mathbf{z}_{t-2})}{\partial c_{t,1} \partial z_{t-2,m}}, \dots, \frac{\partial^2 \log p(\mathbf{c}_t | \mathbf{z}_{t-2})}{\partial c_{t,2n} \partial z_{t-2,m}} \right) \oplus \left(\frac{\partial^3 \log p(\mathbf{c}_t | \mathbf{z}_{t-2})}{\partial c_{t,i} \partial c_{t,j} \partial z_{t-2,m}} \right)_{(i,j) \in \mathcal{E}(\mathcal{M}_{\mathbf{c}_t})}, \quad (5)$$

where \oplus denotes concatenation operation and $(i, j) \in \mathcal{E}(\mathcal{M}_{\mathbf{c}_t})$ denotes all pairwise indice such that $c_{t,i}, c_{t,j}$ are adjacent in $\mathcal{M}_{\mathbf{c}_t}$. For $m \in [1, \dots, n]$, there exist $4n + 2|\mathcal{M}_{\mathbf{c}_t}|$ different values of $\mathbf{z}_{t-2,m}$, as the $4n + 2|\mathcal{M}_{\mathbf{c}_t}|$ values of vector functions $w(m)$ are linearly independent.

Then for any two different entries $\hat{c}_{t,k}, \hat{c}_{t,l} \in \hat{\mathbf{c}}_t$ that are **not adjacent** in the Markov network $\mathcal{M}_{\hat{\mathbf{c}}_t}$ over estimated $\hat{\mathbf{c}}_t$,

- (i) Each ground-truth latent variable $c_{t,i} \in \mathbf{c}_t$ is a function of at most one of \hat{c}_k and \hat{c}_l ,
- (ii) For each pair of ground-truth latent variables $c_{t,i}$ and $c_{t,j}$ that are **adjacent** in $\mathcal{M}_{\mathbf{c}_t}$ over \mathbf{c}_t , they can not be a function of $\hat{c}_{t,k}$ and $\hat{c}_{t,l}$ respectively.

Proof Sketch. The proof can be found in Appendix A2.1. First, we establish a bijective transformation between the ground-truth \mathbf{z}_t and the estimated $\hat{\mathbf{z}}_t$ to connect them together. Next, we utilize the structural properties of the ground-truth Markov network $\mathcal{M}_{\mathbf{c}_t}$ to constrain the structure of the estimated Markov network $\mathcal{M}_{\hat{\mathbf{c}}_t}$ through the connection between conditional independence and cross derivatives[38], i.e., $c_{t,i} \perp c_{t,j} | \mathbf{c}_t \setminus \{c_{t,i}, c_{t,j}\}$ implies $\frac{\partial^2 \log p(\mathbf{c}_t)}{\partial c_{t,i} \partial c_{t,j}} = 0$. By introducing the sufficient variability assumption, we further construct a linear system with a full rank coefficient matrix to ensure that the only solution holds, i.e.,

$$\frac{\partial c_{t,i}}{\partial \hat{c}_{t,k}} \cdot \frac{\partial c_{t,i}}{\partial \hat{c}_{t,l}} = 0, \quad \frac{\partial c_{t,i}}{\partial \hat{c}_{t,k}} \cdot \frac{\partial c_{t,j}}{\partial \hat{c}_{t,l}} = 0, \quad \frac{\partial^2 c_{t,i}}{\partial c_{t,k} \partial c_{t,l}} = 0, \quad (6)$$

where $\frac{\partial c_{t,i}}{\partial \hat{c}_{t,k}} \cdot \frac{\partial c_{t,i}}{\partial \hat{c}_{t,l}} = 0$ and $\frac{\partial c_{t,i}}{\partial \hat{c}_{t,k}} \cdot \frac{\partial c_{t,j}}{\partial \hat{c}_{t,l}} = 0$ correspond to statement (i) statement (ii), respectively.

Discussion. The first assumptions from Theorem 1 are standard in the component-wise identification of existing nonlinear ICA for time series data[39], i.e., the latent variables are changing continuously, which is common in time series data. The second assumption has been commonly adopted for the existing identifiable results of temporally causal representation learning for sufficient changes. Theorem 1 provides an insight, such that when observational equivalence holds, the variables that are directly related in the true Markov network must be functions of directly related variables in the estimated Markov network. Please note that τ and L can be easily generalized to any value by making some modifications on the assumption A2. The τ timestamps that are conditioned on provide sufficient changes, and L sequence length provides a sparse structure, which will be discussed in Theorem 2. A detailed discussion is given in Appendix A2.2.

3.2 Identification of Latent Variables

In this subsection, we demonstrate that given further sparsity assumptions, the latent Markov network over \mathbf{c}_t and the latent variables are also identifiable. For a better explanation of the identifiability of latent variables, we first introduce the definition of the **Intimate Neighbor Set** [36].

Definition 2 (Intimate Neighbor Set [36]). *Consider a Markov network \mathcal{M}_Z over variables set Z , and the intimate neighbor set of variable $z_{t,i}$ is*

$$\Psi_{\mathcal{M}_{\mathbf{c}_t}}(c_{t,i}) \triangleq \{c_{t,j} | c_{t,j} \text{ is adjacent to } c_{t,i}, \text{ and it is also adjacent to all other neighbors of } c_{t,i}, c_{t,j} \in \mathbf{c}_t \setminus \{c_{t,i}\}\}$$

Based on the conclusions of Theorem 1, we consider 3 consecutive timestamps, i.e., $\mathbf{c}_t = \{\mathbf{z}_{t-1}, \mathbf{z}_t, \mathbf{z}_{t+1}\}$, where the identifiability of \mathbf{z}_t can be assured with the help of the contextual information \mathbf{z}_{t-1} and \mathbf{z}_{t+1} .

Theorem 2. (Component-wise Identification of Latent Variables with instantaneous dependencies.) *Suppose that the observations are generated by Equation (1) and (2), and $\mathcal{M}_{\mathbf{c}_t}$ is the Markov network over $\mathbf{c}_t = \{\mathbf{z}_{t-1}, \mathbf{z}_t, \mathbf{z}_{t+1}\}$. Except for the assumptions A1 and A2 from Theorem 1, we further make the following assumption:*

- **A3 (Latent Process Sparsity):** *For any $z_{t,i} \in \mathbf{z}_t$, the intimate neighbor set of $z_{t,i}$ is an empty set.*

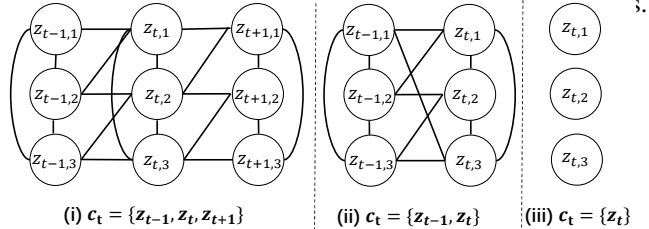
When the observational equivalence is achieved with the minimal number of edges of the estimated Markov network of $\mathcal{M}_{\hat{\mathbf{c}}_t}$, then we have the following two statements:

- The estimated Markov network $\mathcal{M}_{\hat{\mathbf{c}}_t}$ is isomorphic to the ground-truth Markov network $\mathcal{M}_{\mathbf{c}_t}$.*
- There exists a permutation π of the estimated latent variables, such that $z_{t,i}$ and $\hat{z}_{t,\pi(i)}$ is one-to-one corresponding, i.e., $z_{t,i}$ is component-wise identifiable.*

Proof Sketch. Given the fact that there always exists a row permutation for each invertible matrix such that the permuted diagonal entries are non-zero [33], we utilize the conclusion of Theorem 1 to demonstrate that any edge present in the true Markov network will necessarily exist in the estimated one. Furthermore, when the number of estimated edges reaches a minimum, the identifiability of Markov network can be achieved. Finally, we once again leverage Theorem 1 to illustrate that the permutation which allows the Markov network to be identified can further lead to a component-wise level identifiability of latent variables. A detailed proof is given in Appendix A2.3.

Discussion. Intuitively, Theorem 2 tells us that any latent variable $z_{t,i}$ is identifiable when its intimate set is empty, which benefits from the sparse causal influence. Compared with the existing identifiability results for instantaneous dependencies like intervention or grouping observations, this assumption is more practical and reasonable in real-world time series datasets. For instance, in human motion forecasting, the human skeleton is a sparse structure, since the joints in arms and legs are significantly independent

One more thing to note is that it is not necessary to utilize all contextual information for identifiability. In fact, as long as there exist consecutive timestamps where the intimate sets of all variables in \mathbf{z}_t are empty, the identifiability can be established.



Corollary 2.1. (General Case for Component-wise Identification.) *Suppose that the observations are generated by Equation (1) and (2), and there exists $\mathbf{c}_t = \{\mathbf{z}_{t-a}, \dots, \mathbf{z}_t, \dots, \mathbf{z}_{t+b}\}$ with the corresponding Markov network $\mathcal{M}_{\mathbf{c}_t}$. Suppose assumptions A1 and A2 hold true, and for any $z_{t,i} \in \mathbf{z}_t$, the intimate neighbor set of $z_{t,i}$ is an empty set. When the observational equivalence is achieved with the minimal number of edges of*

Figure 2: Examples of Markov networks with different types of contextual information that satisfy the sparse latent process assumption. Case (i) uses both historical and future information for identifiability. Case (ii) uses only historical information. Case (iii) that does not include instantaneous dependencies can identify latent variables without any contextual information, which degenerates to TDRL[39]. Please note that in all cases, we show only the Markov net of \mathbf{c}_t conditioned on previous timestamps while omitting the conditions for simplicity.

estimated Markov network of $\mathcal{M}_{\hat{\epsilon}_t}$, there must exist a permutation π of the estimated latent variables, such that $z_{t,i}$ and $\hat{z}_{t,\pi(i)}$ is one-to-one corresponding, i.e., $z_{t,i}$ is component-wise identifiable.

Discussion. In this part, we give a further discussion on how contextual information can help to identify current latent variables. Let us take Figure 2 (i) as an example, when we consider the current latent variables $z_{t,1}, z_{t,2}$ and $z_{t,3}$ only, it is easy to see that neither $z_{t,1}$ nor $z_{t,3}$ are identifiable since both of their intimate set are $\{z_{t,2}\}$. However, when the historical information \mathbf{z}_{t-1} is taken into consideration, where $z_{t-1,1}$ affects only $z_{t,1}$ but not $z_{t,2}$, then $z_{t,1}$ will immediately be identified since the intimate set of $z_{t,1}$ will be empty thanks to the unique influence from $z_{t-1,1}$. Similarly, with a future variable $z_{t+1,3}$ which is influenced by $z_{t,3}$ but not $z_{t,1}$, then $z_{t,3}$ can be identified as well. Besides, under some circumstances, only part of the contextual information is needed. Therefore, the length of the required time window L can be reduced as well, which leads to a more relaxed requirement of assumption A2, according to Theorem 1. As shown in Figure 2 (ii), with only historical information, the identifiability of \mathbf{z}_t can already be achieved. Furthermore, some existing identifiability results [23, 39] can be considered as a special case of our theoretical results when the instantaneous effects vanish. For example, Figure 2 (iii) provides the example of TDRL [39], where all intimate sets are empty naturally, and the identifiability is assured.

4 Identifiable Instantaneous Latent Dynamic Model

4.1 Temporally Variational Inference Architecture

Based on the data generation process, we derive the evidence lower bound (ELBO) as shown in Equation (6). Appendix A3.2 illustrates the derivation details of the ELBO.

$$ELBO = \underbrace{\mathbb{E}_{q(\mathbf{z}_{1:T}|\mathbf{x}_{1:T})} \ln p(\mathbf{x}_{1:T}|\mathbf{z}_{1:T})}_{L_r} - \alpha \underbrace{D_{KL}(q(\mathbf{z}_{1:T}|\mathbf{x}_{1:T})||p(\mathbf{z}_{1:T}))}_{L_K}, \quad (7)$$

where α denotes the hyper-parameters and D_{KL} denotes the KL divergence. $q(\mathbf{z}_{1:T}|\mathbf{x}_{1:T})$ and $p(\mathbf{x}_{1:T}|\mathbf{z}_{1:T})$ which are used to approximate the prior distribution and reconstruct the observations. Formally, the encoder and the decoder can be formalized as follows.

$$\mathbf{z}_{1:T} = \phi(\mathbf{x}_{1:T}), \quad \hat{\mathbf{x}} = \psi(\mathbf{z}_{1:T}), \quad (8)$$

where ϕ and ψ denote the neural architecture based on convolution neural networks. Based on theoretical results, we develop the **IDOL** model as shown in Figure 3, which is built on the variational inference to model the distribution of observations. To estimate the prior distribution and enforce the independent noise assumption, we devise the prior networks. Moreover, we employ a gradient-based sparsity penalty to promote the sparse causal influence.

4.2 Prior Estimation

To estimate the prior distribution of latent variables, we propose the prior networks. Specifically, we first let r_i be a set of learned inverse transition functions that take the estimated latent variables as input to estimate the noise term $\hat{\epsilon}_i$, i.e. $\hat{\epsilon}_{t,i} = r_i(\hat{\mathbf{z}}_t, \hat{\mathbf{z}}_{t-1})$ ³. And each r_i is implemented by Multi-layer Perceptron networks (MLPs). Sequentially, we devise a transformation $\kappa := \{\hat{\mathbf{z}}_{t-1}, \hat{\mathbf{z}}_t\} \rightarrow \{\hat{\mathbf{z}}_{t-1}, \hat{\epsilon}_t\}$, whose Jacobian can be formalized as $\mathbf{J}_\kappa = \begin{pmatrix} \mathbb{I} & 0 \\ \mathbf{J}_d & \mathbf{J}_e \end{pmatrix}$, where $\mathbf{J}_d = \text{diag}\left(\frac{\partial r_i}{\partial \hat{z}_{t-1,i}}\right)$ and $\mathbf{J}_e = \text{diag}\left(\frac{\partial r_i}{\partial \hat{z}_{t,i}}\right)$. Hence we have Equation (8) via the change of variables formula.

$$\log p(\hat{\mathbf{z}}_t, \hat{\mathbf{z}}_{t-1}) = \log p(\hat{\mathbf{z}}_{t-1}, \epsilon_t) + \log \left| \frac{\partial r_i}{\partial \hat{z}_{t,i}} \right|. \quad (9)$$

³We use the superscript symbol to denote estimated latent variables

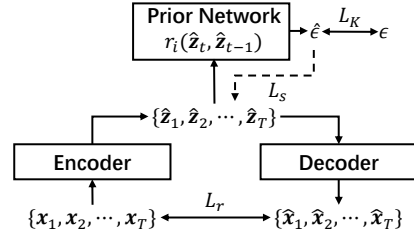


Figure 3: The framework of the **IDOL** model. The encoder and decoder are used for latent variables extraction and observation reconstruction. The prior network is used for prior distribution estimation, and L_s denotes the gradient-based sparsity penalty. The solid and dashed arrows denote the forward and backward propagation, respectively.

According to the generation process, the noise $\epsilon_{t,i}$ is independent with \mathbf{z}_{t-1} , so we can enforce the independence of the estimated noise term $\hat{\epsilon}_{t,i}$. And Equation (8) can be further rewritten as

$$\log p(\hat{\mathbf{z}}_{1:T}) = p(\hat{z}_1) \prod_{\tau=2}^T \left(\sum_{i=1}^n \log p(\hat{\epsilon}_{\tau,i}) + \sum_{i=1}^n \log \left| \frac{\partial r_i}{\partial z_{t,i}} \right| \right), \quad (10)$$

where $p(\hat{\epsilon}_{\tau,i})$ is assumed to follow a Gaussian distribution. Please refer to Appendix A3.1 for more details of the prior derivation.

4.3 Gradient-based Sparsity Regularization

Ideally, the MLPs-based architecture r_i can capture the causal structure of latent variables by restricting the independence of noise $\hat{\epsilon}_{t,i}$. However, without any further constraint, r_i may bring redundant causal edges from $\hat{\mathbf{z}}_{t-1}, \hat{\mathbf{z}}_{t,[n]\setminus i}$ to $\hat{z}_{t,i}$, leading to the incorrect estimation of prior distribution and further the suboptimization of ELBO. As mentioned in Subsection 4.2, \mathbf{J}_d and \mathbf{J}_e intuitively denote the time-delayed and instantaneous causal structures of latent variables, since they describe how the $\hat{\mathbf{z}}_{t-1}, \hat{\mathbf{z}}_{t,[n]\setminus i}$ contribute to $\hat{z}_{t,i}$, which motivate us to remove these redundant causal edges with a sparsity regularization term \mathcal{L}_S by simply applying the \mathcal{L}_1 on \mathbf{J}_d and \mathbf{J}_e . Formally, we have

$$L_S = \|\mathbf{J}_d\|_1 + \|\mathbf{J}_e\|_1, \quad (11)$$

where $\|\cdot\|_1$ denotes the \mathcal{L}_1 Norm of a matrix. By employing the gradient-based sparsity penalty on the estimated latent causal processes, we can indirectly restrict the sparsity of Markov networks to satisfy the sparse latent process. Finally, the total loss of the **IDOL** model can be formalized as:

$$\mathcal{L}_{total} = -\mathcal{L}_r - \alpha\mathcal{L}_K + \beta\mathcal{L}_S, \quad (12)$$

where α, β denote the hyper-parameters.

5 Experiments

5.1 Experiments on Simulation Data

5.1.1 Experimental Setup

Data Generation. We generate the simulated time series data with the fixed latent causal process as introduced in Equations (1)-(2) and Figure 1 (c). To better evaluate the proposed theoretical results, we provide three datasets with an increasing sparsity degree, which are named Dataset A, B, and C, respectively. We further generate a dense dataset with a dense latent process. Please refer to Appendix A4.1.1 for the details of data generation and evaluation metrics.

Baselines. To evaluate the effectiveness of our method, we consider the following compared methods. First, we consider the standard β -VAE [40] and FactorVAE [41], which ignores historical information and auxiliary variables. Moreover, we consider TDRL [39], iVAE [24], TCL [18], PCL [30], and SlowVAE [42], which use temporal information but do not assume instantaneous dependency on latent processes. Finally, we consider the iCITRIS [34] and G-CaRL [35], which are devised for latent causal processes with instantaneous dependencies but require interventions or grouping of observations. As for G-CaRL, we follow the implementation description in the original paper and assign random grouping for observations. As for iCITRIS, we assign a random intervention variable for latent variables. We repeat each method over three random seeds and report the average results.

5.1.2 Results and Discussion

Quantitative Results: Experiment results of the simulation datasets are shown in Table 1. According to the experiment results, we can obtain the following conclusions: 1) we can find that the proposed **IDOL** model achieves the highest MCC performance, reflecting that our method can identify the latent variables under the temporally latent process with instantaneous dependency. 2) our **IDOL** method also outperforms G-CaRL and iCITRIS, which leverage grouping and interventions for identifiability of latent variables with instantaneous dependencies, reflecting that our method does not require a stricter assumption for identifiability. 3) Compared with the existing methods for temporal data like TDRL, PCL, and TCL, the experiment results show that our method can identify the general stationary latent process with instantaneous dependencies. 4) Considering the results of our **IDOL**

Table 1: Experiments results on simulation data.

Datasets	IDOL	TDRL	G-CaRL	iCITRIS	β -VAE	SlowVAE	iVAE	FactorVAE	PCL	TCL
A	0.9142	0.8727	0.6248	0.4120	0.4113	0.2875	0.5545	0.2158	0.5288	0.3311
B	0.9645	0.9416	0.9059	0.8219	0.8485	0.8512	0.6283	0.8512	0.8659	0.8625
C	0.9801	0.9001	0.5850	0.4234	0.4093	0.3420	0.6736	0.2417	0.3981	0.2796
Dense	0.7869	0.7228	0.5835	0.4646	0.4260	0.3986	0.6071	0.2319	0.4659	0.2881

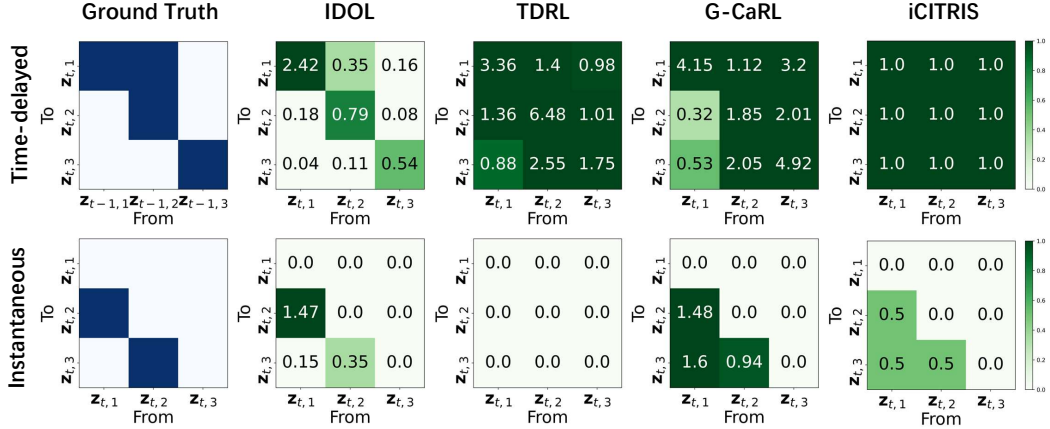


Figure 4: Visualization results of directed acyclic graphs of latent variables of different methods. The first and second rows denote time-delayed and instantaneous causal relationships of latent variables.

method of Dataset A, B, and C with different levels of sparsity, we can find that the more sparse the latent process is, the better identifiable performance the model can achieve, which indirectly reflects the necessity of the sparsity assumption. 5) According to the results of the Dense dataset, the IDOL cannot well identify the latent variables, validating the boundary of our theoretical results.

Qualitative Results: Figure 4 provides visualization results on dataset B of the latent causal process of IDOL, TDRL, G-CaRL, and iCITRIS. Note that the visualization results of our method are generated from \mathbf{J}_d and \mathbf{J}_e . According to the experiment results, we can find that the proposed method can well reconstruct the latent causal relationship, which validates the theoretical results. Moreover, since TDRL employs the conditional independent assumption, it does not reconstruct any instantaneous causal relationships. Besides, without any accurate grouping or intervention information, the G-CaRL and iCITRIS can not reconstruct the correct latent causal relationships. Please refer to Appendix A4.1.4 for more details.

5.2 Experiments on Real-World Data

5.2.1 Experiment Setup

Datasets. To evaluate the effectiveness of our IDOL method in real-world scenarios, we conduct experiments on two human motion datasets: Human3.6M [43] and HumanEva-I [44], which record the location and orientation of local coordinate systems at each joint. We consider these datasets since the joints can be considered as latent variables and they naturally contain instantaneous dependencies. We choose several motions to conduct time series forecasting. For the Human3.6M datasets, we consider 4 motions: Gestures (Ge), Jog (J), CatchThrow (CT), and Walking (W). For HumanEva-I dataset, we consider 6 motions: Discussion (D), Greeting (Gr), Purchases (P), SittingDown (SD), Walking (W), and WalkTogether (WT). For each dataset, we select several motions and partition them into training, validation, and test sets. Please refer the Appendix A4.3 for the dataset descriptions.

Baselines. To evaluate the effectiveness of the proposed IDOL, we consider the following state-of-the-art deep forecasting models for time series forecasting. First, we consider the conventional methods for time series forecasting including Autoformer [45], TimesNet [4] and MICN [46]. Moreover, we consider several latest methods for time series analysis like CARD [47], FITS [48], and iTransformer [49]. Finally, we consider the TDRL [39]. We repeat each experiment over 3 random seeds and publish the average performance. Please refer to Appendix A4.2 for more experiment details.

Table 2: MSE and MAE results on the different motions.

dataset	Predict Length	IDOL		TDRL		CARD		FITS		MICN		iTransformer		TimesNet		Autoformer		
		MSE	MAE	MSE	MAE	MSE	MAE	MSE	MAE	MSE	MAE	MSE	MAE	MSE	MAE	MSE	MAE	
Humanava	G	100	0.0658	0.1623	0.0729	0.1806	0.0898	0.1999	0.0728	0.1758	0.0781	0.1896	0.0905	0.2013	0.0832	0.1949	0.1039	0.2232
		125	0.0809	0.1916	0.0878	0.1993	0.0896	0.1985	0.0834	0.1994	0.0832	0.1990	0.0901	0.2000	0.0830	0.1934	0.1010	0.2195
		150	0.0697	0.1754	0.0724	0.1796	0.0827	0.1894	0.0866	0.1950	0.0715	0.1789	0.0875	0.1965	0.0831	0.1942	0.1006	0.2192
	J	125	0.1516	0.2479	0.2310	0.3392	0.2836	0.3486	0.3277	0.4058	0.1598	0.2587	0.2306	0.3258	0.2189	0.3071	0.3370	0.2532
		150	0.1572	0.2632	0.2333	0.3431	0.3614	0.3936	0.3396	0.4142	0.1648	0.2713	0.2874	0.3673	0.2695	0.3526	0.3367	0.3199
		175	0.1742	0.2786	0.2810	0.3710	0.3938	0.4246	0.3552	0.4329	0.1864	0.2945	0.3074	0.3841	0.3056	0.3707	0.3147	0.2934
	TC	25	0.0060	0.0490	0.0086	0.0607	0.0101	0.0614	0.0116	0.0651	0.0086	0.0607	0.0104	0.0619	0.0147	0.0723	0.0254	0.1043
		50	0.0128	0.0718	0.0151	0.0811	0.0172	0.0801	0.0142	0.0725	0.0158	0.0835	0.0138	0.0711	0.0219	0.0891	0.0263	0.1062
		75	0.0175	0.0844	0.0191	0.0896	0.0228	0.0686	0.0146	0.0729	0.0185	0.0867	0.0136	0.0701	0.0203	0.0869	0.0279	0.1108
	W	25	0.0670	0.1338	0.0968	0.1704	0.1010	0.1641	0.1094	0.2117	0.0967	0.1851	0.0604	0.1344	0.0958	0.1710	0.0940	0.1767
		50	0.1183	0.1814	0.1461	0.2172	0.2387	0.2578	0.2152	0.3089	0.1521	0.2228	0.1245	0.2043	0.1730	0.2389	0.3093	0.3498
		75	0.1977	0.2543	0.2091	0.2642	0.4777	0.3673	0.3156	0.3817	0.2124	0.2706	0.2239	0.2784	0.2202	0.2884	0.3854	0.4009
Human	D	125	0.0071	0.0485	0.0074	0.0509	0.0080	0.0510	0.0085	0.0523	0.0080	0.0524	0.0076	0.0486	0.0097	0.0568	0.0104	0.0586
		250	0.0094	0.0563	0.0096	0.0590	0.0117	0.0600	0.0114	0.0590	0.0107	0.0598	0.0112	0.0581	0.0133	0.0643	0.0134	0.0656
		375	0.0102	0.0638	0.0106	0.0621	0.0138	0.0645	0.0124	0.0615	0.0109	0.0605	0.0126	0.0617	0.0152	0.0675	0.0141	0.0678
	G	125	0.0120	0.0641	0.0167	0.0757	0.0197	0.0763	0.0239	0.0866	0.0144	0.0703	0.0137	0.0649	0.0195	0.0784	0.0217	0.0845
		250	0.0158	0.0808	0.0218	0.0880	0.0283	0.0932	0.0298	0.0982	0.0203	0.0847	0.0217	0.0832	0.0277	0.0933	0.0287	0.0974
		375	0.0226	0.0902	0.0234	0.0914	0.0295	0.0970	0.0304	0.1011	0.0233	0.0912	0.0263	0.0920	0.0311	0.0988	0.0319	0.1029
	P	125	0.0203	0.0778	0.0233	0.0866	0.0247	0.0837	0.0327	0.0987	0.0237	0.0862	0.0228	0.0793	0.0308	0.0939	0.0400	0.1108
		250	0.0296	0.1003	0.0303	0.1060	0.0407	0.1109	0.0426	0.1168	0.0358	0.1146	0.0434	0.1182	0.0554	0.1337	0.0546	0.1361
		375	0.0324	0.1104	0.0333	0.1148	0.0480	0.1268	0.0509	0.1315	0.0364	0.1199	0.0495	0.1312	0.0595	0.1439	0.0638	0.1498
	SD	125	0.0142	0.0709	0.0157	0.0777	0.0175	0.0772	0.0209	0.0889	0.0163	0.0802	0.0162	0.0735	0.0236	0.0948	0.0279	0.1086
		250	0.0250	0.1046	0.0251	0.1050	0.0313	0.1113	0.0331	0.1176	0.0256	0.1069	0.0289	0.1064	0.0355	0.1212	0.0378	0.1302
		375	0.0290	0.1150	0.0301	0.1186	0.0400	0.1296	0.0409	0.1335	0.0300	0.1186	0.0371	0.1246	0.0440	0.1379	0.0441	0.1424
W	125	0.0093	0.0490	0.0102	0.0590	0.0113	0.0616	0.0404	0.0941	0.0111	0.0612	0.0123	0.0610	0.0124	0.0623	0.0682	0.1127	
	250	0.0163	0.0728	0.0166	0.0729	0.0351	0.1033	0.0995	0.1441	0.0173	0.0742	0.0364	0.0981	0.0336	0.0947	0.0881	0.1381	
	375	0.0193	0.0778	0.0207	0.0798	0.0470	0.1188	0.1135	0.1548	0.0206	0.0804	0.0483	0.1126	0.0435	0.1080	0.1219	0.1617	
WT	125	0.0129	0.0667	0.0135	0.0676	0.0195	0.0779	0.0646	0.1244	0.0145	0.0693	0.0180	0.0719	0.0216	0.0787	0.0733	0.1301	
	250	0.0206	0.0815	0.0217	0.0830	0.0449	0.1147	0.1127	0.1623	0.0211	0.0821	0.0437	0.1083	0.0425	0.1058	0.1041	0.1566	
	375	0.0233	0.0873	0.0248	0.0886	0.0552	0.1255	0.1149	0.1641	0.0245	0.0887	0.0474	0.1146	0.0456	0.1122	0.1165	0.1654	

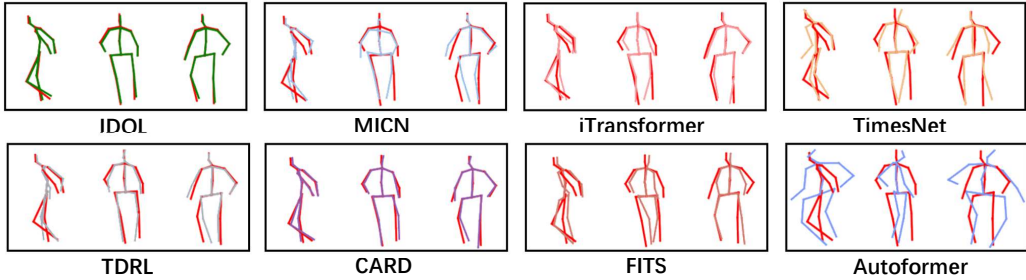


Figure 5: The illustration of visualization of different methods of Walking. The red lines denote the ground-truth motions, those lines in other colors denote the prediction motions of different methods.

5.2.2 Results and Discussion

Quantitative Results: Experiment results of the real-world datasets are shown in Table ???. More experiment results are shown in Appendix A4.4. According to the experiment results, our **IDOL** model significantly outperforms all other baselines on most of the human motion forecasting tasks. Specifically, our method outperforms the most competitive baseline by a clear margin of 4%-34% and promotes the forecasting accuracy substantially on complex motions like the SittingDown (SD) and the Walking (W). This is because the human motion datasets contain more complex patterns described by stable causal structures, and our method can learn the latent causal process with identifiability guarantees. It is noted that our method achieves a better performance than that of TDRL, which does not consider the instantaneous dependencies among latent variables. We also find that our model achieves a comparable performance in the motion of CatchThrow (CT), this is because the size of this dataset is too small for the model to model the distribution of the observations. We further consider a more complex synthetic mixture of human motion forecasting, experiment results are shown in Appendix A4.4. Please refer to Appendix A4.5 for the experiment results of ablation studies.

Qualitative Results: To further show the effectiveness of the proposed method, we also visualize the forecasting results of different models. Visualization results in Figure 5 illustrate how the forecasting results align the ground-truth motions, where the red lines denote the ground-truth motions and the lines in other colors denote the forecasting results of different methods. According to the experiment results, we can find that the forecasting results of our method achieve the best alignment of the ground truth. In the meanwhile, the other methods that do not consider the instantaneous dependencies of latent variables, may generate some exaggerated body movements, for example, the hyperflexed knee

joint and the actions that violate the physics rules, which reflects the importance of considering the instantaneous dependencies of latent causal process of time series data.

6 Conclusion

This paper proposes a general identifiability framework for temporal causal representation learning with instantaneous dependencies. Different from existing methods that require the assumptions of grouping observations and interventions, the proposed **IDOL** model employs the sparse latent process assumption, which is easy to satisfy in real-world time series data. We also devise a variational-inference-based method with sparsity regularization to build the gap between theories and practice. Experiment results on simulation datasets evaluate the effectiveness of latent variables identification and latent directed acyclic graphs reconstruction. Evaluation in human motion datasets with instantaneous dependencies reflects the practicability in real-world scenarios.

References

- [1] Kexin Zhang, Qingsong Wen, Chaoli Zhang, Rongyao Cai, Ming Jin, Yong Liu, James Zhang, Yuxuan Liang, Guansong Pang, Dongjin Song, et al. Self-supervised learning for time series analysis: Taxonomy, progress, and prospects. *arXiv preprint arXiv:2306.10125*, 2023.
- [2] Binh Tang and David S Matteson. Probabilistic transformer for time series analysis. *Advances in Neural Information Processing Systems*, 34:23592–23608, 2021.
- [3] Bing Li, Wei Cui, Le Zhang, Ce Zhu, Wei Wang, Ivor Tsang, and Joey Tianyi Zhou. Diffformer: Multi-resolutional differencing transformer with dynamic ranging for time series analysis. *IEEE Transactions on Pattern Analysis and Machine Intelligence*, 2023.
- [4] Haixu Wu, Tengge Hu, Yong Liu, Hang Zhou, Jianmin Wang, and Mingsheng Long. Timesnet: Temporal 2d-variation modeling for general time series analysis. In *The eleventh international conference on learning representations*, 2022.
- [5] Donghao Luo and Xue Wang. Moderntcn: A modern pure convolution structure for general time series analysis. In *The Twelfth International Conference on Learning Representations*, 2024.
- [6] Kaifeng Bi, Lingxi Xie, Hengheng Zhang, Xin Chen, Xiaotao Gu, and Qi Tian. Accurate medium-range global weather forecasting with 3d neural networks. *Nature*, 619(7970):533–538, 2023.
- [7] Haixu Wu, Hang Zhou, Mingsheng Long, and Jianmin Wang. Interpretable weather forecasting for worldwide stations with a unified deep model. *Nature Machine Intelligence*, 5(6):602–611, 2023.
- [8] Ruey S Tsay. *Analysis of financial time series*. John wiley & sons, 2005.
- [9] Dat Huynh, Elizabeth Fons, and Svitlana Vyetenko. Few-shot learnable augmentation for financial time series prediction under distribution shifts. In *NeurIPS 2022 Workshop on Distribution Shifts: Connecting Methods and Applications*, 2022.
- [10] Jianbo Yang, Minh Nhut Nguyen, Phyo Phyo San, Xiaoli Li, and Shonali Krishnaswamy. Deep convolutional neural networks on multichannel time series for human activity recognition. In *Ijcai*, volume 15, pages 3995–4001. Buenos Aires, Argentina, 2015.
- [11] Yu Kong and Yun Fu. Human action recognition and prediction: A survey. *International Journal of Computer Vision*, 130(5):1366–1401, 2022.
- [12] Haishuai Wang, Qin Zhang, Jia Wu, Shirui Pan, and Yixin Chen. Time series feature learning with labeled and unlabeled data. *Pattern Recognition*, 89:55–66, 2019.
- [13] Ming Jin, Yu Zheng, Yuan-Fang Li, Siheng Chen, Bin Yang, and Shirui Pan. Multivariate time series forecasting with dynamic graph neural odes. *IEEE Transactions on Knowledge and Data Engineering*, 2022.
- [14] Alex Tank, Ian Covert, Nicholas Foti, Ali Shojaie, and Emily B Fox. Neural granger causality. *IEEE Transactions on Pattern Analysis and Machine Intelligence*, 44(8):4267–4279, 2021.
- [15] Zijian Li, Ruichu Cai, Tom ZJ Fu, Zhifeng Hao, and Kun Zhang. Transferable time-series forecasting under causal conditional shift. *IEEE Transactions on Pattern Analysis and Machine Intelligence*, 2023.
- [16] Min Zheng and Samantha Kleinberg. Using domain knowledge to overcome latent variables in causal inference from time series. In *Machine Learning for Healthcare Conference*, pages 474–489. PMLR, 2019.
- [17] Francesco Locatello, Stefan Bauer, Mario Lucic, Gunnar Rätsch, Sylvain Gelly, Bernhard Schölkopf, and Olivier Bachem. A sober look at the unsupervised learning of disentangled representations and their evaluation. *Journal of Machine Learning Research*, 21(209):1–62, 2020.

- [18] Aapo Hyvarinen and Hiroshi Morioka. Unsupervised feature extraction by time-contrastive learning and nonlinear ica. *Advances in neural information processing systems*, 29, 2016.
- [19] Aapo Hyvärinen and Erkki Oja. Independent component analysis: algorithms and applications. *Neural networks*, 13(4-5):411–430, 2000.
- [20] Pierre Comon. Independent component analysis, a new concept? *Signal processing*, 36(3): 287–314, 1994.
- [21] Aapo Hyvärinen. Independent component analysis: recent advances. *Philosophical Transactions of the Royal Society A: Mathematical, Physical and Engineering Sciences*, 371(1984): 20110534, 2013.
- [22] Kun Zhang and Laiwan Chan. Kernel-based nonlinear independent component analysis. In *International Conference on Independent Component Analysis and Signal Separation*, pages 301–308. Springer, 2007.
- [23] Weiran Yao, Yuewen Sun, Alex Ho, Changyin Sun, and Kun Zhang. Learning temporally causal latent processes from general temporal data. *arXiv preprint arXiv:2110.05428*, 2021.
- [24] Ilyes Khemakhem, Diederik Kingma, Ricardo Monti, and Aapo Hyvarinen. Variational autoencoders and nonlinear ica: A unifying framework. In *International Conference on Artificial Intelligence and Statistics*, pages 2207–2217. PMLR, 2020.
- [25] Shaoan Xie, Lingjing Kong, Mingming Gong, and Kun Zhang. Multi-domain image generation and translation with identifiability guarantees. In *The Eleventh International Conference on Learning Representations*, 2022.
- [26] Sébastien Lachapelle, Pau Rodriguez, Yash Sharma, Katie E Everett, Rémi Le Priol, Alexandre Lacoste, and Simon Lacoste-Julien. Disentanglement via mechanism sparsity regularization: A new principle for nonlinear ica. In *Conference on Causal Learning and Reasoning*, pages 428–484. PMLR, 2022.
- [27] Yujia Zheng, Ignavier Ng, and Kun Zhang. On the identifiability of nonlinear ica: Sparsity and beyond. *Advances in Neural Information Processing Systems*, 35:16411–16422, 2022.
- [28] Hermanni H"alv"a and Aapo Hyvarinen. Hidden markov nonlinear ica: Unsupervised learning from nonstationary time series. In *Conference on Uncertainty in Artificial Intelligence*, pages 939–948. PMLR, 2020.
- [29] Hermanni Hälvä, Sylvain Le Corff, Luc LeHéricy, Jonathan So, Yongjie Zhu, Elisabeth Gassiat, and Aapo Hyvarinen. Disentangling identifiable features from noisy data with structured nonlinear ica. *Advances in Neural Information Processing Systems*, 34:1624–1633, 2021.
- [30] Aapo Hyvarinen and Hiroshi Morioka. Nonlinear ica of temporally dependent stationary sources. In *Artificial Intelligence and Statistics*, pages 460–469. PMLR, 2017.
- [31] Aapo Hyvarinen, Hiroaki Sasaki, and Richard Turner. Nonlinear ica using auxiliary variables and generalized contrastive learning. In *The 22nd International Conference on Artificial Intelligence and Statistics*, pages 859–868. PMLR, 2019.
- [32] Ignavier Ng, Yujia Zheng, Xinshuai Dong, and Kun Zhang. On the identifiability of sparse ica without assuming non-gaussianity. *Advances in Neural Information Processing Systems*, 36, 2024.
- [33] Yujia Zheng and Kun Zhang. Generalizing nonlinear ica beyond structural sparsity. *Advances in Neural Information Processing Systems*, 36, 2024.
- [34] Phillip Lippe, Sara Magliacane, Sindy Löwe, Yuki M Asano, Taco Cohen, and Efstratios Gavves. Causal representation learning for instantaneous and temporal effects in interactive systems. In *The Eleventh International Conference on Learning Representations*, 2023.
- [35] Hiroshi Morioka and Aapo Hyvärinen. Causal representation learning made identifiable by grouping of observational variables. *arXiv preprint arXiv:2310.15709*, 2023.

- [36] Kun Zhang, Shaoan Xie, Ignavier Ng, and Yujia Zheng. Causal representation learning from multiple distributions: A general setting. *arXiv preprint arXiv:2402.05052*, 2024.
- [37] Leland Gerson Neuberger. Causality: models, reasoning, and inference, by judea pearl, cambridge university press, 2000. *Econometric Theory*, 19(4):675–685, 2003.
- [38] Juan Lin. Factorizing multivariate function classes. *Advances in neural information processing systems*, 10, 1997.
- [39] Weiran Yao, Guangyi Chen, and Kun Zhang. Temporally disentangled representation learning. *Advances in Neural Information Processing Systems*, 35:26492–26503, 2022.
- [40] Irina Higgins, Loic Matthey, Arka Pal, Christopher P Burgess, Xavier Glorot, Matthew M Botvinick, Shakir Mohamed, and Alexander Lerchner. beta-vae: Learning basic visual concepts with a constrained variational framework. *ICLR (Poster)*, 3, 2017.
- [41] Hyunjik Kim and Andriy Mnih. Disentangling by factorising. In *International conference on machine learning*, pages 2649–2658. PMLR, 2018.
- [42] David Klindt, Lukas Schott, Yash Sharma, Ivan Ustyuzhaninov, Wieland Brendel, Matthias Bethge, and Dylan Paiton. Towards nonlinear disentanglement in natural data with temporal sparse coding. *arXiv preprint arXiv:2007.10930*, 2020.
- [43] Catalin Ionescu, Dragos Papava, Vlad Olaru, and Cristian Sminchisescu. Human3.6m: Large scale datasets and predictive methods for 3d human sensing in natural environments. *IEEE Transactions on Pattern Analysis and Machine Intelligence*, 36(7):1325–1339, 2014. doi: 10.1109/TPAMI.2013.248.
- [44] Leonid Sigal, Alexandru O. Balan, and Michael J. Black. Humaneva: Synchronized video and motion capture dataset and baseline algorithm for evaluation of articulated human motion. *Int. J. Comput. Vis.*, 87(1-2):4–27, 2010. doi: 10.1007/S11263-009-0273-6.
- [45] Haixu Wu, Jiehui Xu, Jianmin Wang, and Mingsheng Long. Autoformer: Decomposition transformers with auto-correlation for long-term series forecasting. *Advances in Neural Information Processing Systems*, 34:22419–22430, 2021.
- [46] Huiqiang Wang, Jian Peng, Feihu Huang, Jince Wang, Junhui Chen, and Yifei Xiao. Micn: Multi-scale local and global context modeling for long-term series forecasting. In *The Eleventh International Conference on Learning Representations*, 2022.
- [47] Xue Wang, Tian Zhou, Qingsong Wen, Jinyang Gao, Bolin Ding, and Rong Jin. Card: Channel aligned robust blend transformer for time series forecasting. In *The Twelfth International Conference on Learning Representations*, 2023.
- [48] Zhijian Xu, Ailing Zeng, and Qiang Xu. FITS: Modeling time series with \$10k\$ parameters. In *The Twelfth International Conference on Learning Representations*, 2024.
- [49] Yong Liu, Tengge Hu, Haoran Zhang, Haixu Wu, Shiyu Wang, Lintao Ma, and Mingsheng Long. itransformer: Inverted transformers are effective for time series forecasting. In *The Twelfth International Conference on Learning Representations*, 2024.
- [50] Goutham Rajendran, Simon Buchholz, Bryon Aragam, Bernhard Schölkopf, and Pradeep Ravikumar. Learning interpretable concepts: Unifying causal representation learning and foundation models. *arXiv preprint arXiv:2402.09236*, 2024.
- [51] Amin Mansouri, Jason Hartford, Yan Zhang, and Yoshua Bengio. Object-centric architectures enable efficient causal representation learning. *arXiv preprint arXiv:2310.19054*, 2023.
- [52] Liang Wendong, Armin Kekić, Julius von Kügelgen, Simon Buchholz, Michel Besserve, Luigi Gresele, and Bernhard Schölkopf. Causal component analysis. *Advances in Neural Information Processing Systems*, 36, 2024.
- [53] Dingling Yao, Danru Xu, Sébastien Lachapelle, Sara Magliacane, Perouz Taslakian, Georg Martius, Julius von Kügelgen, and Francesco Locatello. Multi-view causal representation learning with partial observability. *arXiv preprint arXiv:2311.04056*, 2023.

- [54] Bernhard Schölkopf, Francesco Locatello, Stefan Bauer, Nan Rosemary Ke, Nal Kalchbrenner, Anirudh Goyal, and Yoshua Bengio. Toward causal representation learning. *Proceedings of the IEEE*, 109(5):612–634, 2021.
- [55] Yuejiang Liu, Alexandre Alahi, Chris Russell, Max Horn, Dominik Zietlow, Bernhard Schölkopf, and Francesco Locatello. Causal triplet: An open challenge for intervention-centric causal representation learning. In *2nd Conference on Causal Learning and Reasoning (CLEaR)*, 2023.
- [56] Luigi Gresele, Paul K Rubenstein, Arash Mehrjou, Francesco Locatello, and Bernhard Schölkopf. The incomplete rosetta stone problem: Identifiability results for multi-view nonlinear ica. In *Uncertainty in Artificial Intelligence*, pages 217–227. PMLR, 2020.
- [57] Te-Won Lee and Te-Won Lee. *Independent component analysis*. Springer, 1998.
- [58] Aapo Hyvärinen and Petteri Pajunen. Nonlinear independent component analysis: Existence and uniqueness results. *Neural networks*, 12(3):429–439, 1999.
- [59] Aapo Hyvärinen, Ilyes Khemakhem, and Ricardo Monti. Identifiability of latent-variable and structural-equation models: from linear to nonlinear. *arXiv preprint arXiv:2302.02672*, 2023.
- [60] Ilyes Khemakhem, Ricardo Monti, Diederik Kingma, and Aapo Hyvarinen. Ice-beem: Identifiable conditional energy-based deep models based on nonlinear ica. *Advances in Neural Information Processing Systems*, 33:12768–12778, 2020.
- [61] Zijian Li, Zunhong Xu, Ruichu Cai, Zhenhui Yang, Yuguang Yan, Zhifeng Hao, Guangyi Chen, and Kun Zhang. Identifying semantic component for robust molecular property prediction. *arXiv preprint arXiv:2311.04837*, 2023.
- [62] Lingjing Kong, Shaoan Xie, Weiran Yao, Yujia Zheng, Guangyi Chen, Petar Stojanov, Victor Akinwande, and Kun Zhang. Partial disentanglement for domain adaptation. In *International conference on machine learning*, pages 11455–11472. PMLR, 2022.
- [63] Lingjing Kong, Biwei Huang, Feng Xie, Eric Xing, Yuejie Chi, and Kun Zhang. Identification of nonlinear latent hierarchical models. *arXiv preprint arXiv:2306.07916*, 2023.
- [64] Hanqi Yan, Lingjing Kong, Lin Gui, Yujie Chi, Eric Xing, Yulan He, and Kun Zhang. Counterfactual generation with identifiability guarantees. In *37th International Conference on Neural Information Processing Systems, NeurIPS 2023*, 2023.
- [65] Zijian Li, Ruichu Cai, Guangyi Chen, Boyang Sun, Zhifeng Hao, and Kun Zhang. Subspace identification for multi-source domain adaptation. *Advances in Neural Information Processing Systems*, 36, 2024.
- [66] Danru Xu, Dingling Yao, Sébastien Lachapelle, Perouz Taslakian, Julius von Kügelgen, Francesco Locatello, and Sara Magliacane. A sparsity principle for partially observable causal representation learning. *arXiv preprint arXiv:2403.08335*, 2024.
- [67] Sébastien Lachapelle, Tristan Deleu, Divyat Mahajan, Ioannis Mitliagkas, Yoshua Bengio, Simon Lacoste-Julien, and Quentin Bertrand. Synergies between disentanglement and sparsity: Generalization and identifiability in multi-task learning. In *International Conference on Machine Learning*, pages 18171–18206. PMLR, 2023.
- [68] Sébastien Lachapelle and Simon Lacoste-Julien. Partial disentanglement via mechanism sparsity. *arXiv preprint arXiv:2207.07732*, 2022.
- [69] Sébastien Lachapelle, Pau Rodríguez López, Yash Sharma, Katie Everett, Rémi Le Priol, Alexandre Lacoste, and Simon Lacoste-Julien. Nonparametric partial disentanglement via mechanism sparsity: Sparse actions, interventions and sparse temporal dependencies. *arXiv preprint arXiv:2401.04890*, 2024.
- [70] Zenan Huang, Haobo Wang, Junbo Zhao, and Nenggan Zheng. Latent processes identification from multi-view time series. *arXiv preprint arXiv:2305.08164*, 2023.

- [71] Phillip Lippe, Sara Magliacane, Sindy Löwe, Yuki M Asano, Taco Cohen, and Stratis Gavves. Citris: Causal identifiability from temporal intervened sequences. In *International Conference on Machine Learning*, pages 13557–13603. PMLR, 2022.
- [72] Wei Chen, Zhiyi Huang, Ruichu Cai, Zhifeng Hao, and Kun Zhang. Identification of causal structure with latent variables based on higher order cumulants. In *Proceedings of the AAAI Conference on Artificial Intelligence*, volume 38, pages 20353–20361, 2024.
- [73] Sébastien Lachapelle, Divyat Mahajan, Ioannis Mitliagkas, and Simon Lacoste-Julien. Additive decoders for latent variables identification and cartesian-product extrapolation. *Advances in Neural Information Processing Systems*, 36, 2024.
- [74] Ricardo Pio Monti, Kun Zhang, and Aapo Hyvärinen. Causal discovery with general non-linear relationships using non-linear ica. In *Uncertainty in artificial intelligence*, pages 186–195. PMLR, 2020.
- [75] Kun Zhang and Aapo Hyvarinen. On the identifiability of the post-nonlinear causal model. *arXiv preprint arXiv:1205.2599*, 2012.
- [76] Tatsuya Tashiro, Shohei Shimizu, Aapo Hyvärinen, and Takashi Washio. Estimation of causal orders in a linear non-gaussian acyclic model: a method robust against latent confounders. In *Artificial Neural Networks and Machine Learning–ICANN 2012: 22nd International Conference on Artificial Neural Networks, Lausanne, Switzerland, September 11-14, 2012, Proceedings, Part I 22*, pages 491–498. Springer, 2012.
- [77] Biwei Huang, Charles Jia Han Low, Feng Xie, Clark Glymour, and Kun Zhang. Latent hierarchical causal structure discovery with rank constraints. *Advances in Neural Information Processing Systems*, 35:5549–5561, 2022.
- [78] Lingjing Kong, Biwei Huang, Feng Xie, Eric Xing, Yuejie Chi, and Kun Zhang. Identification of nonlinear latent hierarchical models. *Advances in Neural Information Processing Systems*, 36, 2024.
- [79] Feng Xie, Biwei Huang, Zhengming Chen, Yangbo He, Zhi Geng, and Kun Zhang. Identification of linear non-gaussian latent hierarchical structure. In *International Conference on Machine Learning*, pages 24370–24387. PMLR, 2022.
- [80] Ruichu Cai, Feng Xie, Clark Glymour, Zhifeng Hao, and Kun Zhang. Triad constraints for learning causal structure of latent variables. *Advances in neural information processing systems*, 32, 2019.
- [81] Sudeshna Adak. *Time-dependent spectral analysis of nonstationary time series*. Stanford University, 1996.
- [82] Christos Koutlis, Vasilios K Kimiskidis, and Dimitris Kugiumtzis. Identification of hidden sources by estimating instantaneous causality in high-dimensional biomedical time series. *International Journal of Neural Systems*, 29(04):1850051, 2019.
- [83] W Gersch. Modeling nonstationary time series and inferring instantaneous dependency, feedback and causality: An application to human epileptic seizure event data. *IFAC Proceedings Volumes*, 18(5):737–742, 1985.
- [84] Noor Jamaludeen, Vishnu Unnikrishnan, André Brechmann, and Myra Spiliopoulou. Discovering instantaneous granger causalities in non-stationary categorical time series data. In *International Conference on Artificial Intelligence in Medicine*, pages 200–209. Springer, 2022.
- [85] Anpeng Wu, Haoxuan Li, Kun Kuang, Keli Zhang, and Fei Wu. Hierarchical topological ordering with conditional independence test for limited time series. *arXiv preprint arXiv:2308.08148*, 2023.
- [86] Norman R Swanson and Clive WJ Granger. Impulse response functions based on a causal approach to residual orthogonalization in vector autoregressions. *Journal of the American Statistical Association*, pages 357–367, 1997.

- [87] Aapo Hyvärinen, Kun Zhang, Shohei Shimizu, and Patrik O Hoyer. Estimation of a structural vector autoregression model using non-gaussianity. *Journal of Machine Learning Research*, 11(5), 2010.
- [88] Mingming Gong, Kun Zhang, Bernhard Schoelkopf, Dacheng Tao, and Philipp Geiger. Discovering temporal causal relations from subsampled data. In *International Conference on Machine Learning*, pages 1898–1906. PMLR, 2015.
- [89] Mingming Gong, Kun Zhang, Bernhard Schölkopf, Clark Glymour, and Dacheng Tao. Causal discovery from temporally aggregated time series. In *Uncertainty in artificial intelligence: proceedings of the... conference. Conference on Uncertainty in Artificial Intelligence*, volume 2017. NIH Public Access, 2017.
- [90] Zhengmao Zhu, Yuren Liu, Honglong Tian, Yang Yu, and Kun Zhang. Beware of instantaneous dependence in reinforcement learning. *arXiv preprint arXiv:2303.05458*, 2023.
- [91] Rob J Hyndman and George Athanasopoulos. *Forecasting: principles and practice*. OTexts, 2018.
- [92] George EP Box and David A Pierce. Distribution of residual autocorrelations in autoregressive-integrated moving average time series models. *Journal of the American statistical Association*, 65(332):1509–1526, 1970.
- [93] Sepp Hochreiter and Jürgen Schmidhuber. Long short-term memory. *Neural computation*, 9(8):1735–1780, 1997.
- [94] Guokun Lai, Wei-Cheng Chang, Yiming Yang, and Hanxiao Liu. Modeling long-and short-term temporal patterns with deep neural networks. In *The 41st international ACM SIGIR conference on research & development in information retrieval*, pages 95–104, 2018.
- [95] David Salinas, Valentin Flunkert, Jan Gasthaus, and Tim Januschowski. Deepar: Probabilistic forecasting with autoregressive recurrent networks. *International Journal of Forecasting*, 36(3):1181–1191, 2020.
- [96] Shaojie Bai, J Zico Kolter, and Vladlen Koltun. An empirical evaluation of generic convolutional and recurrent networks for sequence modeling. *arXiv preprint arXiv:1803.01271*, 2018.
- [97] Albert Gu, Karan Goel, Ankit Gupta, and Christopher Ré. On the parameterization and initialization of diagonal state space models. *Advances in Neural Information Processing Systems*, 35:35971–35983, 2022.
- [98] Albert Gu, Isys Johnson, Karan Goel, Khaled Saab, Tri Dao, Atri Rudra, and Christopher Ré. Combining recurrent, convolutional, and continuous-time models with linear state space layers. *Advances in neural information processing systems*, 34:572–585, 2021.
- [99] Albert Gu, Karan Goel, and Christopher Ré. Efficiently modeling long sequences with structured state spaces. *arXiv preprint arXiv:2111.00396*, 2021.
- [100] Haoyi Zhou, Shanghang Zhang, Jieqi Peng, Shuai Zhang, Jianxin Li, Hui Xiong, and Wancai Zhang. Informer: Beyond efficient transformer for long sequence time-series forecasting. In *Proceedings of the AAAI conference on artificial intelligence*, volume 35, pages 11106–11115, 2021.
- [101] Yuqi Nie, Nam H Nguyen, Phanwadee Sinthong, and Jayant Kalagnanam. A time series is worth 64 words: Long-term forecasting with transformers. *arXiv preprint arXiv:2211.14730*, 2022.
- [102] Diederik P Kingma and Jimmy Ba. Adam: A method for stochastic optimization. *arXiv preprint arXiv:1412.6980*, 2014.

Supplement to

“On the Identification of Temporally Causal Representation with Instantaneous Dependence”

Appendix organization:

A1 Related Works	18
A1.1 Identifiability of Causal Representation Learning	18
A1.2 Nonlinear ICA for Time Series Data	18
A1.3 Causal Discovery with Latent Variables	18
A1.4 Instantaneous Dependence of Time Series Data	18
A1.5 Time Series Forecasting	19
A2 Proof of Theory	19
A2.1 Relationships between Ground-truth and Estimated Latent Variables	19
A2.2 Extension to Multiple Lags and Sequence Lengths	21
A2.3 Identifiability of Latent Variables	21
A2.4 General Case for Component-wise Identifications	23
A3 Implementation Details	23
A3.1 Prior Likelihood Derivation	23
A3.2 Evident Lower Bound	24
A3.3 Model Details	24
A4 Experiment Details	24
A4.1 Simulation Experiment	24
A4.1.1 Data Generation Process	24
A4.1.2 Evaluation Metrics	25
A4.1.3 More Simulation Experiment Results	25
A4.1.4 Implementation Details	25
A4.2 Experiment Details	26
A4.3 Real-world Dataset Description	26
A4.4 More Experiments Results	27
A4.5 Ablation Study	27
A5 Limitation	27
A6 Broader Impacts	27

A1 Related Works

A1.1 Identifiability of Causal Representation Learning

To achieve the causal representation [50–52] for time series data, several researchers leverage the independent component analysis (ICA) to recover the latent variables with identification guarantees [53–56]. Conventional methods assume a linear mixing function from the latent variables to the observed variables [20, 21, 57, 22]. To relax the linear assumption, researchers achieve the identifiability of latent variables via nonlinear ICA by using different types of assumptions like auxiliary variables or sparse generation process [27, 58–61]. As for the methods that employ the auxiliary variables, Aapo et al. first achieve the identifiability by assuming the latent sources with exponential family and introducing auxiliary variables e.g., domain indexes, time indexes, and class labels [24, 18, 30, 31]. To further relax the exponential family assumption, Zhang et al. [62, 25, 63, 64, 25] achieve the component-wise identification results for nonlinear ICA with a $2n + 1$ number of auxiliary variables for n latent variables. Recently, Li et al. [65] further relax to $n + 1$ number of auxiliary variables and achieve subspace identifiability. To seek identifiability in an unsupervised manner, researchers employ the assumption of structural sparsity to achieve identifiability [32, 26, 27, 66]. Specifically, Lachapelle et al. [67, 68] proposed mechanism sparsity regularization as an inductive bias to identify the causal latent factors and achieve the identifiability on several scenarios like multi-task learning. They further show the identifiability results up to the consistency relationship [69], which allows the partial disentanglement of latent variables. Recently, Zhang et al. [36] use the sparse structures of latent variables to achieve identifiability under distribution shift. Different from these methods that assume sparsity exists in the generation process between the latent source and the observation, we assume the *latent process sparsity*, where sparsity exists in the transition of latent variables and is common in real-world time series data dependencies.

A1.2 Nonlinear ICA for Time Series Data

Our work is also related to the temporally causal representation. Existing methods for temporally causal representation [64, 70, 28, 71] usually rely on the conditional independence assumption, where the latent variables are mutually independent conditional on their time-delayed parents. Specifically, Aapo et al. [18] leverage the independent sources principle and the variability of data segments to achieve identifiability on nonstationary time series data. They further use permutation-based contrastive [30] to achieve identifiability on stationary time series data. The recent advancements in temporally causal representation include LEAP [23], TDRL [39], which leverage the properties of independent noises and variability historical information. However, this assumption is too strong to meet in real-world scenarios since instantaneous dependencies are common in real-world scenarios like human motion. To solve this problem, researchers introduce further assumptions. For example, Lippe et al. [34] propose the i-Citris, which demonstrates identifiability by assuming interventions on latent variables. And Morioka et al. [35] propose G-CaRL, which yields identifiability with the assumption of the grouping of observational variables. However, these assumptions are still hard to meet in practice. Hence we propose a more relaxed assumption, transition sparsity, to achieve identifiability under time series data with instantaneous

A1.3 Causal Discovery with Latent Variables

Several studies are proposed to discover causally related latent variables [72–76]. Specifically, Huang et al. [77, 78] leverage the vanishing Tetrad conditions or rank constraints to identify latent variables in linear-Gaussian models. Cai et al. [79, 80] further draw upon non-Gaussianity in their analysis for linear, non-Gaussian scenarios. Other methods aim to reconstruct the hierarchical structures of the latent variables, like [79, 77]. However, these methods usually use the linear assumption and can hardly handle the real-world time series data with complex nonlinear relationships.

A1.4 Instantaneous Dependency of Time Series Data

When the discrete time series data is sampled in a low-frequency or low-resolution manner, instantaneous dependence [81–85] occurs where variables at each time step are not independent given their historical observations. [86] first discuss the instantaneous dependence from the perspective of noise. Lots of works investigate instantaneous dependency from the causal view. Specifically, Hyvärinen

et al. [87] estimate both instantaneous and lagged effects via a non-Gaussian model. Gong et al. [88, 89] discover causal structure with instantaneous dependency from subsampled and aggregated data. Recently, Zhu et al. [90] consider instantaneous dependency in reinforcement learning.

A1.5 Time Series Forecasting

Time series forecasting [91, 92] is one of the most popular research problems in recent years. Recently, the deep-learning-based methods have made great progress, which can be categorized according to different types of neural architectures like the RNN-based methods [93–95], CNN-based models [96, 46, 4], and the methods based on state-space model [97–99]. Recently, Transformer-based methods [100, 45, 101] further push the development of time series forecasting. However, these methods seldom consider the instantaneous dependencies of time series data.

A2 Proof of Theory

A2.1 Relationships between Ground-truth and Estimated Latent Variables

Theorem A1. *For a series of observations $\mathbf{x}_t \in \mathbb{R}^n$ and estimated latent variables $\hat{\mathbf{z}}_t \in \mathbb{R}^n$ with the corresponding process $\hat{f}_i, \hat{p}(\epsilon), \hat{g}$, where \hat{g} is invertible, suppose the process subject to observational equivalence $\mathbf{x}_t = \hat{\mathbf{g}}(\hat{\mathbf{z}}_t)$. Let $\mathbf{c}_t \triangleq \{\mathbf{z}_{t-1}, \mathbf{z}_t\}$ and $\mathcal{M}_{\mathbf{c}_t}$ be the variable set of 2 consecutive timestamps and the corresponding Markov network respectively. Suppose assumptions*

- *A1 (Smooth and Positive Density): The probability function of the latent variables \mathbf{c}_t is smooth and positive, i.e., $p_{\mathbf{c}_t}$ is third order differentiable and $p_{\mathbf{c}_t} > 0$ over \mathbb{R}^{2n} ,*
- *A2 (Sufficient Variability): Denote $|\mathcal{M}_{\mathbf{c}_t}|$ as the number of edges in Markov network $\mathcal{M}_{\mathbf{c}_t}$. Let*

$$w(m) = \left(\frac{\partial^3 \log p(\mathbf{c}_t | \mathbf{z}_{t-2})}{\partial c_{t,1}^2 \partial z_{t-2,m}}, \dots, \frac{\partial^3 \log p(\mathbf{c}_t | \mathbf{z}_{t-2})}{\partial c_{t,2n}^2 \partial z_{t-2,m}} \right) \oplus \left(\frac{\partial^2 \log p(\mathbf{c}_t | \mathbf{z}_{t-2})}{\partial c_{t,1} \partial z_{t-2,m}}, \dots, \frac{\partial^2 \log p(\mathbf{c}_t | \mathbf{z}_{t-2})}{\partial c_{t,2n} \partial z_{t-2,m}} \right) \oplus \left(\frac{\partial^3 \log p(\mathbf{c}_t | \mathbf{z}_{t-2})}{\partial c_{t,i} \partial c_{t,j} \partial z_{t-2,m}} \right)_{(i,j) \in \mathcal{E}(\mathcal{M}_{\mathbf{c}_t})}, \quad (13)$$

where \oplus denotes concatenation operation and $(i, j) \in \mathcal{E}(\mathcal{M}_{\mathbf{c}_t})$ denotes all pairwise indice such that $c_{t,i}, c_{t,j}$ are adjacent in $\mathcal{M}_{\mathbf{c}_t}$. For $m \in [1, \dots, n]$, there exist $4n + 2|\mathcal{M}_{\mathbf{c}_t}|$ different values of $\mathbf{z}_{t-2,m}$, as the $4n + 2|\mathcal{M}_{\mathbf{c}_t}|$ values of vector functions $w(m)$ are linearly independent,

hold true. Then for any two different entries $\hat{c}_{t,k}, \hat{c}_{t,l} \in \hat{\mathbf{c}}_t$ that are **not adjacent** in the Markov network $\mathcal{M}_{\hat{\mathbf{c}}_t}$ over estimated $\hat{\mathbf{c}}_t$,

- (i) Each ground-truth latent variable $c_{t,i} \in \mathbf{c}_t$ is a function of at most one of $\hat{c}_{t,k}$ and $\hat{c}_{t,l}$,
- (ii) For each pair of ground-truth latent variables $c_{t,i}$ and $c_{t,j}$ that are **adjacent** in $\mathcal{M}_{\mathbf{c}_t}$ over \mathbf{c}_t , they can not be a function of $\hat{c}_{t,k}$ and $\hat{c}_{t,l}$ respectively.

Proof. We start from the matched marginal distribution to develop the relationship between \mathbf{z}_t and $\hat{\mathbf{z}}_t$ as follows:

$$p(\hat{\mathbf{x}}_t) = p(\mathbf{x}_t) \iff p(\hat{\mathbf{g}}(\hat{\mathbf{z}}_t)) = p(g(\mathbf{z}_t)) \iff p((g^{-1} \circ \hat{\mathbf{g}})(\hat{\mathbf{z}}_t)) = p(\mathbf{z}_t) \iff p(h_z(\hat{\mathbf{z}}_t)) = p(\mathbf{z}_t), \quad (14)$$

where $\hat{\mathbf{g}} : \mathcal{Z} \rightarrow \mathcal{X}$ denotes the estimated mixing function, and $h := g^{-1} \circ \hat{\mathbf{g}}$ is the transformation between the ground-truth latent variables and the estimated ones. Since $\hat{\mathbf{g}}$ and g are invertible, h is invertible as well. Since Equation 14 holds true for all time steps, there must exist an invertible function h_c such that $p(h_c(\hat{\mathbf{c}}_t)) = p(\mathbf{c}_t)$, whose Jacobian matrix at time step t is

$$\mathbf{J}_{h_c,t} = \begin{bmatrix} \mathbf{J}_{h_z,t-1} & 0 \\ 0 & \mathbf{J}_{h_z,t} \end{bmatrix}. \quad (15)$$

Then for each value of \mathbf{x}_{t-2} , the Jacobian matrix of the mapping from $(\mathbf{x}_{t-2}, \hat{\mathbf{c}}_t)$ to $(\mathbf{x}_{t-2}, \mathbf{c}_t)$ can be written as follows:

$$\begin{bmatrix} \mathbf{I} & \mathbf{0} \\ * & \mathbf{J}_{h_c,t} \end{bmatrix},$$

where $*$ denotes any matrix. Since \mathbf{x}_{t-2} can be fully characterized by itself, the left top and right top block are $\mathbf{1}$ and $\mathbf{0}$ respectively, and the determinant of this Jacobian matrix is the same as $|\mathbf{J}_{h_c,t}|$. Therefore, we have:

$$p(\hat{\mathbf{c}}_t, \mathbf{x}_{t-2}) = p(\mathbf{c}_t, \mathbf{x}_{t-2})|\mathbf{J}_{h_c,t}|. \quad (16)$$

Dividing both sides of Equation (7) by $p(\mathbf{x}_{t-2})$, we further have:

$$p(\hat{\mathbf{c}}_t|\mathbf{x}_{t-2}) = p(\mathbf{c}_t|\mathbf{x}_{t-2})|\mathbf{J}_{h_c,t}|. \quad (17)$$

Since $p(\mathbf{c}_t|\mathbf{x}_{t-2}) = p(\mathbf{c}_t|g(\mathbf{z}_{t-2})) = p(\mathbf{c}_t|\mathbf{z}_{t-2})$, and similarly $p(\hat{\mathbf{c}}_t|\mathbf{x}_{t-2}) = p(\hat{\mathbf{c}}_t|\hat{\mathbf{z}}_{t-2})$, we have:

$$\log p(\hat{\mathbf{c}}_t|\hat{\mathbf{z}}_{t-2}) = \log p(\mathbf{c}_t|\mathbf{z}_{t-2}) + \log |\mathbf{J}_{h_c,t}|. \quad (18)$$

Let $\hat{c}_{t,k}, \hat{c}_{t,l}$ be two different variables that are not adjacent in the estimated Markov network $\mathcal{M}_{\hat{\mathbf{c}}_t}$ over $\hat{\mathbf{c}}_t = \{\hat{\mathbf{z}}_{t-1}, \hat{\mathbf{z}}_t\}$. We conduct the first-order derivative w.r.t. $\hat{c}_{t,k}$ and have

$$\frac{\partial \log p(\hat{\mathbf{c}}_t|\hat{\mathbf{z}}_{t-2})}{\partial \hat{c}_{t,k}} = \sum_{i=1}^{2n} \frac{\partial \log p(\mathbf{c}_t|\mathbf{z}_{t-2})}{\partial c_{t,i}} \cdot \frac{\partial c_{t,i}}{\partial \hat{c}_{t,k}} + \frac{\partial \log |\mathbf{J}_{h_c,t}|}{\partial \hat{c}_{t,k}}. \quad (19)$$

We further conduct the second-order derivative w.r.t. $\hat{c}_{t,k}$ and $\hat{c}_{t,l}$, then we have:

$$\begin{aligned} \frac{\partial \log p(\hat{\mathbf{c}}_t|\hat{\mathbf{z}}_{t-2})}{\partial \hat{c}_{t,k} \partial \hat{c}_{t,l}} &= \sum_{i=1}^{2n} \sum_{j=1}^{2n} \frac{\partial^2 \log p(\mathbf{c}_t|\mathbf{z}_{t-2})}{\partial c_{t,i} \partial c_{t,j}} \cdot \frac{\partial c_{t,i}}{\partial \hat{c}_{t,k}} \cdot \frac{\partial c_{t,j}}{\partial \hat{c}_{t,l}} \\ &+ \sum_{i=1}^{2n} \frac{\partial \log p(\mathbf{c}_t|\mathbf{z}_{t-2})}{\partial c_{t,i}} \cdot \frac{\partial^2 c_{t,i}}{\partial \hat{c}_{t,k} \partial \hat{c}_{t,l}} + \frac{\partial \log |\mathbf{J}_{h_c,t}|}{\partial \hat{c}_{t,k} \partial \hat{c}_{t,l}}. \end{aligned} \quad (20)$$

Since $\hat{c}_{t,k}, \hat{c}_{t,l}$ are not adjacent in $\mathcal{M}_{\hat{\mathbf{c}}_t}$, $\hat{c}_{t,k}$ and $\hat{c}_{t,l}$ are conditionally independent given $\hat{\mathbf{c}}_t \setminus \{\hat{c}_{t,k}, \hat{c}_{t,l}\}$. Utilizing the fact that conditional independence can lead to zero cross derivative [38], for each value of $\hat{\mathbf{z}}_{t-2}$, we have

$$\begin{aligned} \frac{\partial^2 \log p(\hat{\mathbf{c}}_t|\hat{\mathbf{z}}_{t-2})}{\partial \hat{c}_{t,k} \partial \hat{c}_{t,l}} &= \frac{\partial^2 \log p(\hat{c}_{t,k}|\hat{\mathbf{c}}_t \setminus \{\hat{c}_{t,k}, \hat{c}_{t,l}\}, \hat{\mathbf{z}}_{t-2})}{\partial \hat{c}_{t,k} \partial \hat{c}_{t,l}} + \frac{\partial^2 \log p(\hat{c}_{t,l}|\mathbf{c}_t \setminus \{\hat{c}_{t,k}, \hat{c}_{t,l}\}, \hat{\mathbf{z}}_{t-2})}{\partial \hat{c}_{t,k} \partial \hat{c}_{t,l}} \\ &+ \frac{\partial^2 \log p(\hat{\mathbf{c}}_t \setminus \{\hat{c}_{t,k}, \hat{c}_{t,l}\}|\hat{\mathbf{z}}_{t-2})}{\partial \hat{c}_{t,k} \partial \hat{c}_{t,l}} = 0. \end{aligned} \quad (21)$$

Bring in Equation 21, Equation 20 can be further derived as

$$\begin{aligned} 0 &= \underbrace{\sum_{i=1}^{2n} \frac{\partial^2 \log p(\mathbf{c}_t|\mathbf{z}_{t-2})}{\partial c_{t,i}^2} \cdot \frac{\partial c_{t,i}}{\partial \hat{c}_{t,k}} \cdot \frac{\partial c_{t,i}}{\partial \hat{c}_{t,l}}}_{(i) \ i=j} + \underbrace{\sum_{i=1}^{2n} \sum_{(j,i) \in \mathcal{E}(\mathcal{M}_{\mathbf{c}_t})} \frac{\partial^2 \log p(\mathbf{c}_t|\mathbf{z}_{t-2})}{\partial c_{t,i} \partial c_{t,j}} \cdot \frac{\partial c_{t,i}}{\partial \hat{c}_{t,k}} \cdot \frac{\partial c_{t,j}}{\partial \hat{c}_{t,l}}}_{(ii) \ c_{t,i} \text{ and } c_{t,j} \text{ are adjacent in } \mathcal{M}_{\mathbf{c}_t}} \\ &+ \underbrace{\sum_{i=1}^{2n} \sum_{(j,i) \notin \mathcal{E}(\mathcal{M}_{\mathbf{c}_t})} \frac{\partial^2 \log p(\mathbf{c}_t|\mathbf{z}_{t-2})}{\partial c_{t,i} \partial c_{t,j}} \cdot \frac{\partial c_{t,i}}{\partial \hat{c}_{t,k}} \cdot \frac{\partial c_{t,j}}{\partial \hat{c}_{t,l}}}_{(iii) \ c_{t,i} \text{ and } c_{t,j} \text{ are not adjacent in } \mathcal{M}_{\mathbf{c}_t}} \\ &+ \sum_{i=1}^{2n} \frac{\partial \log p(\mathbf{c}_t|\mathbf{z}_{t-2})}{\partial c_{t,i}} \cdot \frac{\partial^2 c_{t,i}}{\partial \hat{c}_{t,k} \partial \hat{c}_{t,l}} + \frac{\partial \log |\mathbf{J}_{h_c,t}|}{\partial \hat{c}_{t,k} \partial \hat{c}_{t,l}}. \end{aligned} \quad (22)$$

Similar to Equation 21, we have $\frac{\partial^2 p(\mathbf{c}_t|\mathbf{z}_{t-2})}{\partial c_{t,i} \partial c_{t,j}} = 0$ when $c_{t,i}, c_{t,j}$ are not adjacent in $\mathcal{M}_{\mathbf{c}_t}$. Thus, Equation 22 can be rewritten as

$$\begin{aligned} 0 &= \sum_{i=1}^{2n} \frac{\partial^2 \log p(\mathbf{c}_t|\mathbf{z}_{t-2})}{\partial c_{t,i}^2} \cdot \frac{\partial c_{t,i}}{\partial \hat{c}_{t,k}} \cdot \frac{\partial c_{t,i}}{\partial \hat{c}_{t,l}} + \sum_{i=1}^{2n} \sum_{(j,i) \in \mathcal{E}(\mathcal{M}_{\mathbf{c}_t})} \frac{\partial^2 \log p(\mathbf{c}_t|\mathbf{z}_{t-2})}{\partial c_{t,i} \partial c_{t,j}} \cdot \frac{\partial c_{t,i}}{\partial \hat{c}_{t,k}} \cdot \frac{\partial c_{t,j}}{\partial \hat{c}_{t,l}} \\ &+ \sum_{i=1}^{2n} \frac{\partial \log p(\mathbf{c}_t|\mathbf{z}_{t-2})}{\partial c_{t,i}} \cdot \frac{\partial^2 c_{t,i}}{\partial \hat{c}_{t,k} \partial \hat{c}_{t,l}} + \frac{\partial \log |\mathbf{J}_{h_c,t}|}{\partial \hat{c}_{t,k} \partial \hat{c}_{t,l}}. \end{aligned} \quad (23)$$

Then for each $m = 1, 2, \dots, n$ and each value of $z_{t-2,m}$, we conduct partial derivative on both sides of Equation 23 and have:

$$0 = \sum_{i=1}^{2n} \frac{\partial^3 \log p(\mathbf{c}_t | \mathbf{z}_{t-2})}{\partial c_{t,i}^2 \partial z_{t-2,m}} \cdot \frac{\partial c_{t,i}}{\partial \hat{c}_{t,k}} \cdot \frac{\partial c_{t,i}}{\partial \hat{c}_{t,l}} + \sum_{i=1}^{2n} \sum_{(j,i) \in \mathcal{E}(\mathcal{M}_c)} \frac{\partial^3 \log p(\mathbf{c}_t | \mathbf{z}_{t-2})}{\partial c_{t,i} \partial c_{t,j} \partial z_{t-2,m}} \cdot \frac{\partial c_{t,i}}{\partial \hat{c}_{t,k}} \cdot \frac{\partial c_{t,j}}{\partial \hat{c}_{t,l}} + \sum_{i=1}^{2n} \frac{\partial^2 \log p(c_t | \mathbf{z}_{t-2})}{\partial c_{t,i} \partial z_{t-2,m}} \cdot \frac{\partial c_{t,i}^2}{\partial \hat{c}_{t,k} \partial \hat{c}_{t,l}}, \quad (24)$$

According to Assumption A2, we can construct $4n + 2|\mathcal{M}_c|$ different equations with different values of $z_{t-2,m}$, and the coefficients of the equation system they form are linearly independent. To ensure that the right-hand side of the equations are always 0, the only solution is

$$\frac{\partial c_{t,i}}{\partial \hat{c}_{t,k}} \cdot \frac{\partial c_{t,i}}{\partial \hat{c}_{t,l}} = 0, \quad (25)$$

$$\frac{\partial c_{t,i}}{\partial \hat{c}_{t,k}} \cdot \frac{\partial c_{t,j}}{\partial \hat{c}_{t,l}} = 0, \quad (26)$$

$$\frac{\partial c_{t,i}^2}{\partial \hat{c}_{t,k} \partial \hat{c}_{t,l}} = 0. \quad (27)$$

According to the aforementioned results, for any two different entries $\hat{c}_{t,k}, \hat{c}_{t,l} \in \hat{\mathbf{c}}_t$ that are **not adjacent** in the Markov network $\mathcal{M}_{\hat{\mathbf{c}}_t}$ over estimated $\hat{\mathbf{c}}_t$, we draw the following conclusions.

(i) Equation 25 implies that, each ground-truth latent variable $c_{t,i} \in \mathbf{c}_t$ is a function of at most one of $\hat{c}_{t,k}$ and $\hat{c}_{t,l}$,

(ii) Equation 26 implies that, for each pair of ground-truth latent variables $c_{t,i}$ and $c_{t,j}$ that are **adjacent** in $\mathcal{M}_{\mathbf{c}_t}$ over \mathbf{c}_t , they can not be a function of $\hat{c}_{t,k}$ and $\hat{c}_{t,l}$ respectively. \square

A2.2 Extension to Multiple Lags and Sequence Lengths

For the sake of simplicity, we consider only one special case with $\tau = 1$ and $L = 2$ in Theorem A2. Our identifiability theorem can be actually extended to arbitrary lags and subsequences easily. For any given τ , and subsequence which is centered at \mathbf{z}_t with previous lo and following hi steps, i.e., $\mathbf{c}_t = \{\mathbf{z}_{t-lo}, \dots, \mathbf{z}_t, \dots, \mathbf{z}_{t+hi}\}$. In this case, the vector function $w(i, j, m)$ in Sufficient Variability Assumption should be modified as

$$w(i, j, m) = \left(\frac{\partial^3 \log p(\mathbf{c}_t | \mathbf{z}_{t-lo-1}, \dots, \mathbf{z}_{t-lo-\tau})}{\partial c_{t,1}^2 \partial z_{t-lo-1,m}}, \dots, \frac{\partial^3 \log p(\mathbf{c}_t | \mathbf{z}_{t-lo-1}, \dots, \mathbf{z}_{t-lo-\tau})}{\partial c_{t,2n}^2 \partial z_{t-lo-1,m}} \right) \oplus \left(\frac{\partial^2 \log p(c_t | \mathbf{z}_{t-lo-1}, \dots, \mathbf{z}_{t-lo-\tau})}{\partial c_{t,1} \partial z_{t-lo-1,m}}, \dots, \frac{\partial^2 \log p(c_t | \mathbf{z}_{t-lo-1}, \dots, \mathbf{z}_{t-lo-\tau})}{\partial c_{t,2n} \partial z_{t-lo-1,m}} \right) \oplus \left(\frac{\partial^3 \log p(\mathbf{c}_t | \mathbf{z}_{t-lo-1}, \dots, \mathbf{z}_{t-lo-\tau})}{\partial c_{t,i} \partial c_{t,j} \partial z_{t-lo-1,m}} \right)_{(i,j) \in \mathcal{E}(\mathcal{M}_{\mathbf{c}_t})}. \quad (28)$$

Besides, $2 * (lo + hi + 1) + 2|\mathcal{M}_{\mathbf{c}_t}|$ values of linearly independent vector functions in $z_{t',m}$ for $t' \in [t-lo-1, \dots, t-lo-\tau]$ and $m \in [1, \dots, n]$ are required as well. The rest part of the theorem remains the same, and the proof can be easily extended in such a setting.

A2.3 Identifiability of Latent Variables

Theorem A2. (Component-wise Identification of Latent Variables with instantaneous dependencies.) Suppose that the observations are generated by Equation 1 and 2, and $\mathcal{M}_{\mathbf{c}_t}$ is the Markov network over $\mathbf{c}_t = \{\mathbf{z}_{t-1}, \mathbf{z}_t, \mathbf{z}_{t+1}\}$. Except for the assumptions A1 and A2 from Theorem 1, we further make the following assumption:

- A3 (Sparse Latent Process): For any $z_{t,i} \in \mathbf{z}_t$, the intimate neighbor set of $z_{t,i}$ is an empty set.

When the observational equivalence is achieved with the minimal number of edges of estimated Markov network of $\mathcal{M}_{\hat{c}_t}$, then we have the following two statements:

- (i) The estimated Markov network $\mathcal{M}_{\hat{c}_t}$ is isomorphic to the ground-truth Markov network \mathcal{M}_{c_t} .
- (ii) There exists a permutation π of the estimated latent variables, such that $z_{t,i}$ and $\hat{z}_{t,\pi(i)}$ is one-to-one corresponding, i.e., $z_{t,i}$ is component-wise identifiable.

Proof. First, we demonstrate that there always exists a row permutation for each invertible matrix such that the permuted diagonal entries are non-zero [36]. By contradiction, if the product of the diagonal entry of an invertible matrix A is zero for every row permutation, then we have Equation

$$\det(A) = \sum_{\sigma \in \mathcal{S}_n} \left(\text{sgn}(\sigma) \prod_{i=1}^n a_{\sigma(i),i} \right), \quad (29)$$

by the Leibniz formula, where \mathcal{S}_n is the set of n -permutations. Thus, we have

$$\prod_{i=1}^n a_{\sigma(i),i} = 0, \quad \forall \sigma \in \mathcal{S}_n, \quad (30)$$

which indicates that $\det(A) = 0$ and A is non-invertible. It contradicts the assumption that A is invertible, and a row permutation where the permuted diagonal entries are non-zero must exist. Since h_z is invertible, there exists a permuted version of the estimated latent variables, denoted as $\hat{\mathbf{z}}_t^\pi$, such that

$$\frac{\partial z_{t,i}}{\partial \hat{z}_{t,\pi(i)}} \neq 0, \quad i = 1, \dots, n. \quad (31)$$

Since $\mathbf{c}_t = \{\mathbf{z}_{t-1}, \mathbf{z}_t, \mathbf{z}_{t+1}\}$, by applying π on each timestamp, we have π' such that

$$\frac{\partial c_{t,i}}{\partial \hat{c}_{t,\pi'(i)}} \neq 0, \quad i = 1, \dots, 3n. \quad (32)$$

Second, we demonstrate that \mathcal{M}_{c_t} is identical to $\mathcal{M}_{\hat{c}_t^{\pi'}}$, where $\mathcal{M}_{\hat{c}_t^{\pi'}}$ denotes the Markov network of the permuted version of $\mathbf{c}_t^{\pi'}$.

On the one hand, for any pair of (i, j) such that $c_{t,i}, c_{t,j}$ are **adjacent** in \mathcal{M}_{c_t} while $c_{t,\pi'(i)}, c_{t,\pi'(j)}$ are **not adjacent** in $\mathcal{M}_{\hat{c}_t^{\pi'}}$, according to Equation 26, we have $\frac{\partial c_{t,i}}{\partial c_{t,\pi'(i)}} \cdot \frac{\partial c_{t,j}}{\partial c_{t,\pi'(j)}} = 0$, which is a contradiction with how π' is constructed. Thus, any edge presents in \mathcal{M}_{c_t} must exist in $\mathcal{M}_{\hat{c}_t^{\pi'}}$. On the other hand, since observational equivalence can be achieved by the true latent process (g, f, p_{c_t}) , the true latent process is clearly the solution with minimal edges.

Under the sparsity constraint on the edges of $\mathcal{M}_{\hat{c}_t^{\pi'}}$, the permuted estimated Markov network $\mathcal{M}_{\hat{c}_t^{\pi'}}$ must be identical to the true Markov network \mathcal{M}_{c_t} . Thus, we claim that

- (i) the estimated Markov network $\mathcal{M}_{\hat{c}_t}$ is isomorphic to the ground-truth Markov network \mathcal{M}_{c_t} .

Sequentially, we further give the proof that under the same permutation \mathbf{z}_t^π (which corresponds to $\mathbf{c}_t^{\pi'}$), $z_{t,i}$ is only the function of $z_{t,\pi(i)}$. Since the permutation happens on each timestamp respectively, the cross-timestamp disentanglement is prevented clearly.

Now let us focus on instantaneous disentanglement. Suppose there exists a pair of indices $i, j \in [1, \dots, n]$. According to Equation 31, we have $\frac{\partial z_{t,i}}{\partial \hat{z}_{t,\pi(i)}} = 0$ and $\frac{\partial z_{t,j}}{\partial \hat{z}_{t,\pi(j)}} = 0$. Let us discuss it case by case.

- If $z_{t,i}$ is not adjacent to $z_{t,j}$, we have $\hat{z}_{t,\pi(i)}$ is not adjacent to $\hat{z}_{t,\pi(j)}$ as well according to the conclusion of identical Markov network. Using Equation 25, we have $\frac{\partial z_{t,i}}{\partial \hat{z}_{t,\pi(i)}} \cdot \frac{\partial z_{t,i}}{\partial \hat{z}_{t,\pi(j)}} = 0$, which leads to $\frac{\partial z_{t,i}}{\partial \hat{z}_{t,\pi(j)}} = 0$.
- If $z_{t,i}$ is adjacent to $z_{t,j}$, we have $\hat{z}_{t,\pi(i)}$ is adjacent to $\hat{z}_{t,\pi(j)}$. When the Latent Process Sparsity assumption is assured, i.e., the intimate neighbor set of $z_{t,i}$ is empty, there exists at

least one index k such that $z_{t,k}$ is adjacent to $z_{t,i}$ but not adjacent to $z_{t,j}$. Similarly, we have the same structure on the estimated Markov network, which means that $\hat{z}_{t,\pi(k)}$ is adjacent to $\hat{z}_{t,\pi(i)}$ but not adjacent to $\hat{z}_{t,\pi(j)}$. Using Equation 26 we have $\frac{\partial z_{t,k}}{\partial \hat{z}_{t,\pi(k)}} \cdot \frac{\partial z_{t,i}}{\partial \hat{z}_{t,\pi(i)}} = 0$, which leads to $\frac{\partial z_{t,i}}{\partial \hat{z}_{t,\pi(j)}} = 0$.

In conclusion, we always have $\frac{\partial z_{t,i}}{\partial \hat{z}_{t,\pi(j)}} = 0$. Thus, we have reached the conclusion that

(ii) there exists a permutation π of the estimated latent variables, such that $z_{t,i}$ and $\hat{z}_{t,\pi(i)}$ is one-to-one corresponding, i.e., $z_{t,i}$ is component-wise identifiable. □

A2.4 General Case for Component-wise Identifications

In this part, we briefly give the proof for a more general case of our theorem.

Corollary A1. (General Case for Component-wise Identification.) *Suppose that the observations are generated by Equation 1 and 2, and there exists $\mathbf{c}_t = \{\mathbf{z}_{t-a}, \dots, \mathbf{z}_t, \dots, \mathbf{z}_{t+b}\}$ with the corresponding Markov network $\mathcal{M}_{\mathbf{c}_t}$. Suppose assumptions A1 and A2 hold true, and for any $z_{t,i} \in \mathbf{z}_t$, the intimate neighbor set of $z_{t,i}$ is an empty set. When the observational equivalence is achieved with the minimal number of edges of estimated Markov network of $\mathcal{M}_{\mathbf{c}_t}$, there must exist a permutation π of the estimated latent variables, such that $z_{t,i}$ and $\hat{z}_{t,\pi(i)}$ is one-to-one corresponding, i.e., $z_{t,i}$ is component-wise identifiable.*

Proof. The proof is similar to that of Theorem A2. The only difference is that given a different subsequence, the variables that are used to make intimate neighbors empty might be different. The rest part of the theorem remains the same. □

Here we further discuss the idea behind the Sparse Latent Process. For two latent variables $z_{t,i}, z_{t,j}$ that are entangled at some certain timestamp, the contextual information can be utilized to recover these variables. Intuitively speaking, when $z_{t,i}$ is directly affected by some previous variable, says $z_{t-1,k}$, while $z_{t,j}$ is not. In this case, the changes that happen on $z_{t-1,k}$ can be captured, which helps to tell $z_{t,i}$ from $z_{t,j}$. Similarly, if $z_{t,i}$ directly affects $z_{t+1,k}$ while $z_{t,j}$ does not, we can distinguish $z_{t,i}$ from $z_{t,j}$ as well. When all variables are naturally conditionally independent, no contextual information will be needed. One more thing to note is that, even though the sparse latent process is not fully satisfied, as long as some structures mentioned above exist, the corresponding entanglement can be prevented.

A3 Implementation Details

A3.1 Prior Likelihood Derivation

We first consider the prior of $\ln p(\mathbf{z}_{1:t})$. We start with an illustrative example of stationary latent causal processes with two time-delay latent variables, i.e. $\mathbf{z}_t = [z_{t,1}, z_{t,2}]$ with maximum time lag $L = 1$, i.e., $z_{t,i} = f_i(\mathbf{z}_{t-1}, \epsilon_{t,i})$ with mutually independent noises. Then we write this latent process as a transformation map \mathbf{f} (note that we overload the notation f for transition functions and for the transformation map):

$$\begin{bmatrix} z_{t-1,1} \\ z_{t-1,2} \\ z_{t,1} \\ z_{t,2} \end{bmatrix} = \mathbf{f} \left(\begin{bmatrix} z_{t-1,1} \\ z_{t-1,2} \\ \epsilon_{t,1} \\ \epsilon_{t,2} \end{bmatrix} \right).$$

By applying the change of variables formula to the map \mathbf{f} , we can evaluate the joint distribution of the latent variables $p(z_{t-1,1}, z_{t-1,2}, z_{t,1}, z_{t,2})$ as

$$p(z_{t-1,1}, z_{t-1,2}, z_{t,1}, z_{t,2}) = \frac{p(z_{t-1,1}, z_{t-1,2}, \epsilon_{t,1}, \epsilon_{t,2})}{|\det \mathbf{J}_{\mathbf{f}}|}, \quad (33)$$

where \mathbf{J}_f is the Jacobian matrix of the map \mathbf{f} , where the instantaneous dependencies are assumed to be a low-triangular matrix:

$$\mathbf{J}_f = \begin{bmatrix} 1 & 0 & 0 & 0 \\ 0 & 1 & 0 & 0 \\ \frac{\partial z_{t,1}}{\partial z_{t-1,1}} & \frac{\partial z_{t,1}}{\partial z_{t-1,2}} & \frac{\partial z_{t,1}}{\partial \epsilon_{t,1}} & 0 \\ \frac{\partial z_{t,2}}{\partial z_{t-1,1}} & \frac{\partial z_{t,2}}{\partial z_{t-1,2}} & \frac{\partial z_{t,2}}{\partial \epsilon_{t,1}} & \frac{\partial z_{t,2}}{\partial \epsilon_{t,2}} \end{bmatrix}.$$

Given that this Jacobian is triangular, we can efficiently compute its determinant as $\prod_i \frac{\partial z_{t,i}}{\epsilon_{t,i}}$. Furthermore, because the noise terms are mutually independent, and hence $\epsilon_{t,i} \perp \epsilon_{t,j}$ for $j \neq i$ and $\epsilon_t \perp \mathbf{z}_{t-1}$, so we can with the RHS of Equation (33) as follows

$$p(z_{t-1,1}, z_{t-1,2}, z_{t,1}, z_{t,2}) = p(z_{t-1,1}, z_{t-1,2}) \times \frac{p(\epsilon_{t,1}, \epsilon_{t,2})}{|\mathbf{J}_f|} = p(z_{t-1,1}, z_{t-1,2}) \times \frac{\prod_i p(\epsilon_{t,i})}{|\mathbf{J}_f|}. \quad (34)$$

Finally, we generalize this example and derive the prior likelihood below. Let $\{r_i\}_{i=1,2,3,\dots}$ be a set of learned inverse transition functions that take the estimated latent causal variables, and output the noise terms, i.e., $\hat{\epsilon}_{t,i} = r_i(\hat{\mathbf{z}}_{t,i}, \{\hat{\mathbf{z}}_{t-\tau}\})$. Then we design a transformation $\mathbf{A} \rightarrow \mathbf{B}$ with low-triangular Jacobian as follows:

$$\underbrace{[\hat{\mathbf{z}}_{t-L}, \dots, \hat{\mathbf{z}}_{t-1}, \hat{\mathbf{z}}_t]^\top}_{\mathbf{A}} \text{ mapped to } \underbrace{[\hat{\mathbf{z}}_{t-L}, \dots, \hat{\mathbf{z}}_{t-1}, \hat{\epsilon}_{t,i}]^\top}_{\mathbf{B}}, \text{ with } \mathbf{J}_{\mathbf{A} \rightarrow \mathbf{B}} = \begin{bmatrix} \mathbb{I}_{n_s \times L} & 0 \\ * & \text{diag}\left(\frac{\partial r_{i,j}}{\partial \hat{z}_{t,j}}\right) \end{bmatrix}. \quad (35)$$

Similar to Equation (34), we can obtain the joint distribution of the estimated dynamics subspace as:

$$\log p(\mathbf{A}) = \underbrace{\log p(\hat{\mathbf{z}}_{t-L}, \dots, \hat{\mathbf{z}}_{t-1}) + \sum_{i=1}^{n_s} \log p(\hat{\epsilon}_{t,i})}_{\text{Because of mutually independent noise assumption}} + \log(|\det(\mathbf{J}_{\mathbf{A} \rightarrow \mathbf{B}})|) \quad (36)$$

Finally, we have:

$$\log p(\hat{\mathbf{z}}_t | \{\hat{\mathbf{z}}_{t-\tau}\}_{\tau=1}^L) = \sum_{i=1}^{n_s} p(\hat{\epsilon}_{t,i}) + \sum_{i=1}^{n_s} \log \left| \frac{\partial r_i}{\partial \hat{z}_{t,i}} \right| \quad (37)$$

Since the prior of $p(\hat{\mathbf{z}}_{t+1:T} | \hat{\mathbf{z}}_{1:t}) = \prod_{i=t+1}^T p(\hat{\mathbf{z}}_i | \hat{\mathbf{z}}_{i-1})$ with the assumption of first-order Markov assumption, we can estimate $p(\hat{\mathbf{z}}_{t+1:T} | \hat{\mathbf{z}}_{1:t})$ in a similar way.

A3.2 Evident Lower Bound

In this subsection, we show the evident lower bound. We first factorize the conditional distribution according to the Bayes theorem.

$$\begin{aligned} \ln p(\mathbf{x}_{1:T}) &= \ln \frac{p(\mathbf{x}_{1:T}, \mathbf{z}_{1:T})}{p(\mathbf{z}_{1:T} | \mathbf{x}_{1:T})} = \mathbb{E}_{q(\mathbf{z}_{1:T} | \mathbf{x}_{1:T})} \ln \frac{p(\mathbf{x}_{1:T}, \mathbf{z}_{1:T}) q(\mathbf{z}_{1:T} | \mathbf{x}_{1:T})}{p(\mathbf{z}_{1:T} | \mathbf{x}_{1:T}) q(\mathbf{z}_{1:T} | \mathbf{x}_{1:T})} \\ &\geq \underbrace{\mathbb{E}_{q(\mathbf{z}_{1:T} | \mathbf{x}_{1:T})} \ln p(\mathbf{x}_{1:T} | \mathbf{z}_{1:T})}_{L_r} - \underbrace{D_{KL}(q(\mathbf{z}_{1:T} | \mathbf{x}_{1:T}) || p(\mathbf{z}_{1:T}))}_{L_{KLD}} = ELBO \end{aligned} \quad (38)$$

A3.3 Model Details

We choose MICN [46] as the encoder backbone of our model on real-world datasets. Specifically, given the MICN extract the hidden feature, we apply a variational inference block and then a MLP-based decoder. Architecture details of the proposed method are shown in Table A1.

A4 Experiment Details

A4.1 Simulation Experiment

A4.1.1 Data Generation Process

As for the temporally latent processes, we use MLPs with the activation function of LeakyReLU to model the sparse time-delayed and instantaneous relationships of temporally latent variables.

Table A1: Architecture details. T , length of time series. $|\mathbf{x}_t|$: input dimension. n : latent dimension. LeakyReLU: Leaky Rectified Linear Unit. Tanh: Hyperbolic tangent function.

Configuration	Description	Output
ϕ	Latent Variable Encoder	
Input: $\mathbf{x}_{1:t}$	Observed time series	Batch Size $\times t \times \mathbf{x}$ dimension
Dense	$ \mathbf{x}_t $ neurons	Batch Size $\times t \times \mathbf{x}_t $
Concat zero	concatenation	Batch Size $\times T \times \mathbf{x}_t $
Dense	n neurons	Batch Size $\times T \times n$
ψ	Decoder	
Input: $\mathbf{z}_{1:T}$	Latent Variable	Batch Size $\times T \times n$
Dense	$ \mathbf{x}_t $ neurons, Tanh	Batch Size $\times T \times \mathbf{x}_t $
r	Modular Prior Networks	
Input: $\mathbf{z}_{1:T}$	Latent Variable	Batch Size $\times (n+1)$
Dense	128 neurons, LeakyReLU	$(n+1) \times 128$
Dense	128 neurons, LeakyReLU	128×128
Dense	128 neurons, LeakyReLU	128×128
Dense	1 neuron	Batch Size $\times 1$
Jacobian Compute	Compute $\log(\det(J))$	Batch Size

Table A2: Variance results on simulation data.

Datasets	IDOL	TDRL	G-CaRL	iCRITIS	β -VAE	SlowVAE	iVAE	FactorVAE	PCL	TCL
A	0.013	0.022	0.004	0.039	0.013	0.005	0.011	0.035	0.073	0.028
B	0.029	0.045	0.003	0.105	0.014	0.025	0.064	0.025	0.011	0.008
C	0.002	0.028	0.003	0.039	0.031	0.010	0.024	0.027	0.021	0.038
Dense	0.037	0.005	0.001	0.021	0.015	0.002	0.009	0.002	0.039	0.016

Moreover, each independent noise $\epsilon_{t,i}$ is sampled from the distribution of normal distributions. We further let the data generation process from latent variables to observed variables be MLPs with the LeakyReLU units.

We provide 4 synthetic datasets. Dataset A has 5 dimensions and a relatively dense latent causal process, which still satisfies the sparsity assumption. Dataset B has 3 dimension, whose latent causal process is shown in Figure 4. Dataset C has 8 dimensions, in which $z_{i,t}$ affects $z_{i,t+1}$ and $z_{i+1,t}$ (if applicable) only. Dataset Dense has 8 dimensions as well, with a fully connected time-delayed transition and link instantaneous effects.

A4.1.2 Evaluation Metrics.

To evaluate the identifiability performance of our method under instantaneous dependencies, we employ the Mean Correlation Coefficient (MCC) between the ground-truth \mathbf{z}_t and the estimated $\hat{\mathbf{z}}_t$. A higher MCC denotes a better identification performance the model can achieve. In addition, we also draw the estimated latent causal process to validate our method.

A4.1.3 More Simulation Experiment Results

We run each experiment 3 times, with seeds 769, 770, 771. Variance results of the simulation datasets are shown in Table A2.

A4.1.4 Implementation Details

For the implementation of baseline models, we utilized publicly released code for TDRL and iCRITIS. However, since the author did not release the code for G-CaRL, we implemented it ourselves based on the paper.

It is important to note that the original code of iCRITIS only accepts images as input. To adapt it to our needs, we replaced the encoder and decoder with a Variational Autoencoder, with the same hyperparameters used in IDOL.

Table A3: MSE and MAE results of different methods on the transformed HumanEva-I dataset.

dataset	Predict Length	IDOL		TDRL		CARD		FITS		MICN		iTransformer		TimesNet		Autoformer	
		MSE	MAE	MSE	MAE	MSE	MAE	MSE	MAE	MSE	MAE	MSE	MAE	MSE	MAE	MSE	MAE
D	125	0.082	0.196	0.084	0.202	0.127	0.251	0.108	0.237	0.083	0.201	0.106	0.227	0.111	0.235	0.133	0.267
	250	0.101	0.226	0.134	0.274	0.204	0.319	0.141	0.273	0.107	0.236	0.161	0.287	0.192	0.312	0.188	0.326
	375	0.113	0.244	0.144	0.288	0.230	0.342	0.180	0.306	0.115	0.247	0.193	0.315	0.226	0.344	0.224	0.352
G	125	0.091	0.220	0.097	0.235	0.098	0.227	0.168	0.305	0.095	0.225	0.097	0.223	0.117	0.247	0.141	0.283
	250	0.103	0.254	0.139	0.285	0.144	0.274	0.183	0.320	0.130	0.272	0.123	0.260	0.134	0.271	0.154	0.300
	375	0.138	0.276	0.155	0.296	0.179	0.310	0.182	0.321	0.154	0.295	0.146	0.286	0.165	0.308	0.161	0.308
P	125	1.195	0.680	1.337	0.834	1.531	0.787	2.306	1.027	1.259	0.786	1.488	0.793	1.905	0.911	2.941	1.210
	250	1.961	1.045	2.411	1.307	3.124	1.346	3.221	1.293	2.498	1.346	3.152	1.383	3.908	1.513	4.169	1.633
	375	2.326	1.164	2.514	1.326	3.948	1.558	4.020	1.537	2.377	1.274	4.075	1.631	4.315	1.662	4.951	1.815
SD	125	0.365	0.405	0.373	0.418	0.512	0.482	0.595	0.543	0.379	0.425	0.517	0.490	0.523	0.501	0.785	0.632
	250	0.551	0.526	0.573	0.540	0.874	0.671	0.923	0.710	0.569	0.532	0.813	0.655	0.815	0.656	1.061	0.769
	375	0.649	0.579	0.653	0.581	0.980	0.720	1.075	0.781	0.655	0.587	0.959	0.721	0.966	0.726	1.193	0.826
W	125	0.045	0.162	0.047	0.164	0.122	0.254	0.288	0.431	0.046	0.162	0.124	0.257	0.067	0.184	0.314	0.405
	250	0.104	0.256	0.143	0.302	0.333	0.434	0.589	0.618	0.141	0.302	0.340	0.438	0.170	0.292	0.629	0.614
	375	0.150	0.313	0.167	0.331	0.431	0.508	0.691	0.673	0.175	0.341	0.425	0.506	0.253	0.370	1.048	0.761
WT	125	0.062	0.189	0.078	0.214	0.118	0.262	0.227	0.385	0.071	0.204	0.115	0.256	0.131	0.271	0.223	0.361
	250	0.127	0.277	0.152	0.311	0.297	0.421	0.407	0.520	0.153	0.312	0.287	0.414	0.195	0.338	0.935	0.509
	375	0.151	0.305	0.171	0.328	0.365	0.473	0.425	0.530	0.169	0.327	0.313	0.441	0.289	0.431	0.430	0.538

Table A4: Standard deviation of MSE and MAE results on the different motion.

dataset	Predict Length	IDOL		TDRL		CARD		FITS		MICN		iTransformer		TimesNet		Autoformer		
		MSE	MAE	MSE	MAE	MSE	MAE	MSE	MAE									
H36M	G	100	0.0008	0.0004	0.0018	0.0026	0.0008	0.0010	0.0008	0.0010	0.0007	0.0027	0.0016	0.0019	0.0038	0.0049	0.0008	0.0015
		125	0.0009	0.0012	0.0009	0.0010	0.0006	0.0008	0.0005	0.0008	0.0017	0.0033	0.0008	0.0009	0.0004	0.0015	0.0012	0.0012
		150	0.0021	0.0022	0.0026	0.0029	0.0004	0.0005	0.0002	0.0003	0.0002	0.0008	0.0001	0.0003	0.0033	0.0023	0.0012	0.0011
	J	125	0.0144	0.0217	0.0115	0.0085	0.0499	0.0263	0.0026	0.0004	0.0032	0.0081	0.0256	0.0131	0.0872	0.0296	0.0238	0.0171
		150	0.0099	0.0161	0.0088	0.0083	0.0108	0.0050	0.0023	0.0010	0.0106	0.0135	0.0183	0.0116	0.0837	0.0325	0.0085	0.0089
		175	0.0003	0.0038	0.0126	0.0123	0.0478	0.0130	0.0030	0.0010	0.0088	0.0129	0.0355	0.0200	0.0289	0.0109	0.0603	0.0133
	TC	25	0.0001	0.0005	0.0009	0.0028	0.0009	0.0034	0.0009	0.0022	0.0001	0.0010	0.0001	0.0004	0.0015	0.0023	0.0026	0.0055
		50	0.0004	0.0022	0.0011	0.0023	0.0018	0.0038	0.0003	0.0010	0.0003	0.0013	0.0001	0.0004	0.0017	0.0046	0.0021	0.0042
		75	0.0005	0.0026	0.0007	0.0022	0.0019	0.0030	0.0001	0.0002	0.0004	0.0015	0.0002	0.0004	0.0029	0.0078	0.0031	0.0066
W	25	0.0019	0.0039	0.0016	0.0020	0.0053	0.0046	0.0061	0.0069	0.0005	0.0012	0.0018	0.0015	0.0023	0.0027	0.0887	0.0796	
	50	0.0003	0.0009	0.0020	0.0019	0.0432	0.0136	0.0009	0.0004	0.0005	0.0005	0.0022	0.0023	0.0064	0.0078	0.0660	0.0419	
	75	0.0154	0.0217	0.0011	0.0019	0.0630	0.0131	0.0033	0.0025	0.0009	0.0014	0.0033	0.0017	0.0320	0.0169	0.0499	0.0349	
HumanEva-I	D	125	0.0002	0.0028	0.0011	0.0015	0.0012	0.0020	0.0013	0.0013	0.0010	0.0017	0.0015	0.0015	0.0048	0.0037	0.0007	0.0008
		250	0.0012	0.0016	0.0024	0.0024	0.0067	0.0038	0.0002	0.0005	0.0010	0.0013	0.0009	0.0006	0.0128	0.0089	0.0044	0.0042
		375	0.0056	0.0062	0.0001	0.0009	0.0109	0.0064	0.0003	0.0004	0.0020	0.0026	0.0033	0.0021	0.0063	0.0012	0.0043	0.0030
	G	125	0.0043	0.0090	0.0066	0.0111	0.0026	0.0030	0.0058	0.0050	0.0064	0.0105	0.0053	0.0054	0.0016	0.0019	0.0076	0.0066
		250	0.0095	0.0174	0.0105	0.0147	0.0093	0.0059	0.0027	0.0022	0.0016	0.0021	0.0063	0.0071	0.0006	0.0018	0.0003	0.0002
		375	0.0014	0.0017	0.0005	0.0006	0.0059	0.0034	0.0013	0.0004	0.0037	0.0047	0.0085	0.0079	0.0035	0.0036	0.0046	0.0043
	P	125	0.0311	0.0277	0.0951	0.0434	0.0465	0.0229	0.0169	0.0062	0.0333	0.0277	0.0251	0.0032	0.2698	0.0744	0.0700	0.0013
		250	0.0719	0.0225	0.0601	0.0318	0.1735	0.0154	0.0317	0.0086	0.0155	0.0069	0.0123	0.0024	0.5525	0.0976	0.0708	0.0093
		375	0.2728	0.0168	0.0889	0.0335	0.1108	0.0319	0.0051	0.0907	0.0382	0.0171	0.0222	0.0034	0.0472	0.0040	0.0880	0.0243
	SD	125	0.0056	0.0031	0.0119	0.0116	0.0045	0.0038	0.0043	0.0027	0.0157	0.0155	0.0131	0.0099	0.0219	0.0167	0.0362	0.0235
		250	0.0024	0.0002	0.0075	0.0077	0.0415	0.0176	0.0008	0.0011	0.0229	0.0146	0.0064	0.0029	0.0172	0.0069	0.0061	0.0017
		375	0.0149	0.0145	0.0072	0.0079	0.0107	0.0044	0.0025	0.0014	0.0050	0.0020	0.0110	0.0057	0.0105	0.0051	0.0336	0.0100
	W	125	0.0029	0.0043	0.0078	0.0150	0.0034	0.0041	0.0037	0.0039	0.0016	0.0034	0.0062	0.0087	0.0028	0.0032	0.1585	0.1221
		250	0.0082	0.0105	0.0236	0.0300	0.0157	0.0127	0.0002	0.0006	0.0125	0.0142	0.0130	0.0101	0.0105	0.0107	0.1344	0.0748
		375	0.0089	0.0108	0.0273	0.0296	0.0035	0.0053	0.0019	0.0014	0.0212	0.0225	0.0121	0.0088	0.0081	0.0067	0.2889	0.0771
	WT	125	0.0031	0.0029	0.0065	0.0106	0.0059	0.0066	0.0032	0.0035	0.0019	0.0022	0.0021	0.0027	0.0056	0.0042	0.0453	0.0455
		250	0.0014	0.0030	0.0044	0.0066	0.0123	0.0102	0.0007	0.0010	0.0054	0.0085	0.0113	0.0111	0.0554	0.0523	0.0168	0.0152
		375	0.0146	0.0188	0.0020	0.0027	0.0431	0.0283	0.0019	0.0014	0.0029	0.0027	0.0077	0.0054	0.0328	0.0246	0.0054	0.0043

When calculating the MCC for all methods, we use the mean value from the VAE encoder. Regarding the latent causal graph, we employ different approaches depending on the method. For IDOL, TDRL, and G-CaRL, we utilize the Jacobian matrix as a proxy for capturing the causal process. On the other hand, for iCRITIS, we rely on the "get_adj_matrix()" function provided in its original code to obtain the latent causal graph.

A4.2 Experiment Details.

We use ADAM optimizer [102] in all experiments and report the mean squared error (MSE) and the mean absolute error (MAE) as evaluation metrics. All experiments are implemented by Pytorch on a single NVIDIA RTX A100 40GB GPU.

A4.3 Real-world Dataset Description

Human3.6M Dataset is collected over 3.6 million different human poses, viewed from 4 different angles, using an accurate human motion capture system. The motions were executed by 11 professional actors, and cover a diverse set of everyday scenarios including conversations, eating, greeting, talking on the phone, posing, sitting, smoking, taking photos, waiting, walking in various non-typical scenarios. We randomly use four motions, i.e., Gestures (Ge), Jog (J), CatchThrow (CT), and Walking (W), for the task of the human motion forecasting. The data is obtained from the

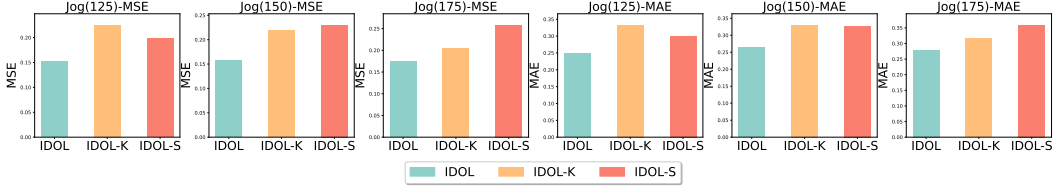


Figure A1: Ablation study on the Jog motion. we explore the impact of different loss terms.

joint angles (provided by Vicon’s skeleton fitting procedure) by applying forward kinematics on the skeleton of the subject. The parametrization is called relative because there is a specially designated joint, usually called the root (roughly corresponding to the pelvis bone position), which is taken as the center of the coordinate system, while the other joints are estimated relative to it.

In this dataset, the joint positions can be considered as latent variables. And the kinematic representation can be considered as the observed variables. The kinematic representation (KR) considers the relative joint angles between limbs. We consider the process from joint position to joint angles as a mixture process.

HumanEva-I dataset comprises 3 subjects each performing several action categories. Each pose has 15 joints with three axis. We choose 6 motions, i.e., : Discussion (D), Greeting (Gr), Purchases (P), SittingDown (SD), Walking (W), and WalkTogether (WT) for the task of human motion forecasting. Specifically, the ground truth motion of the body was captured using a commercial motion capture (MoCap) system from ViconPeak.5 The system uses reflective markers and six 1M-pixel cameras to recover the 3D position of the markers and thereby estimate the 3D articulated pose of the body. We consider the joints as latent variables and the signals recorded from the system as observations.

A4.4 More Experiments Results

We further consider a more complex mixture process. To achieve is, we further apply a transformation on the observed variables, i.e., $\bar{\mathbf{x}}_t = f_o(\mathbf{x}_t)$, where f_o is a linear transformation. Then we can consider the sensors as latent variables with instantaneous dependencies and conduct motion forecasting on the transformed datasets. Experiment results on the transformed HumanEva-I dataset are shown in Table A3.

A4.5 Ablation Study

To evaluate the effectiveness of individual loss terms, we also devise the two model variants. 1) **IDOL-K**: remove the KL divergence restriction of prior estimation. 2) **IDOL-S**: remove sparsity restriction of latent dynamics. Experiment results on the Jog dataset are shown in Figure A1. We can find that the sparsity restriction of latent dynamics plays an important role in the model performance, reflecting that the restriction of latent dynamics can benefit the identifiability of latent variables. We also discover that incorporating the KL divergence has a positive impact on the overall performance of the model, which shows the necessity of identifiability.

A5 Limitation

The proposed method can hardly be applied in the high-dimensional time series data. Therefore, how to relax this restriction and make it scalable to the high-dimensional real-world datasets would be a meaningful future direction.

A6 Broader Impacts

The proposed **IDOL** identifies the latent variables to create a transparent model with a certain degree of interpretability, thereby revealing the causal mechanism of general time series data.